

A direct simulation approach for the Poisson-Boltzmann equation using the Random Batch Method

Lei Li^{*1}, Jian-Guo Liu^{†2}, and Yijia Tang^{‡3}

¹School of Mathematical Sciences, Institute of Natural Sciences, MOE-LSC,
Shanghai Jiao Tong University, Shanghai, 200240, P. R. China.

²Department of Mathematics and Department of Physics, Duke University,
Durham, NC 27708, USA.

³School of Mathematical Sciences, Shanghai Jiao Tong University, Shanghai,
200240, P. R. China.

Abstract

The Poisson-Boltzmann equation is a nonlinear elliptic equation that describes how electronic potential changes in the screening layer when a cell is immersed in an ionic solution. It is the equilibrium state formed by many charged particles interacting with each other through Coulomb forces. We propose a direct simulation approach for the dynamics of the charged particles in the solution governed by the Poisson-Nernst-Planck equation and the Poisson-Boltzmann equation can be solved automatically when the particles reach the equilibrium. The interacting N particle system is simulated in the truncated external domain. Directly simulating the N particle system has an $\mathcal{O}(N^2)$ computational cost in each time step. By making use of the Random Batch Method (RBM) proposed by Jin et al [J. Comput. Phys., 400(1): 108877, 2020], the cost per time step is reduced remarkably to $\mathcal{O}(N)$. Another benefit of RBM is that the hard sphere potential is no longer needed in the simulation. An error analysis is provided for the truncation and numerical experiments are performed to validate the method. This particle method is preferable in two aspects: it is simple and effective in high dimensions, especially in non-symmetric cases or with complicated membrane or molecular surface. Meanwhile, direct simulation may be preferred as people may be interested in the dynamics of the physical process.

1 Introduction

The Poisson-Boltzmann (PB) equation describes the electrostatic phenomena of electrolyte solutions. It was proposed by Gouy [13] and Chapman [4] independently. The PB equation has a wide range of applications in electrochemistry [13, 4], biophysics [16, 8] and colloidal physics. It is valid to describe the distribution of the electric potential in dilute solution at equilibrium state when a charged surface is present. When an object with free charges inside is immersed into an ionic solution, diffuse layers of ions are formed due to thermal motion. The charged object might be a solid particle, a cell, a macromolecule, a gas bubble, a liquid droplet, or porous media[1]. As for the ion transport, the Poisson-Nernst-Planck (PNP) equations [10, 28, 18] can be taken into account to describe the non-equilibrium processes. Other Poisson-Boltzmann type equations such as the charge conserved Poisson-Boltzmann (CCPB) equation [23, 24] have been widely studied as well.

^{*}leili2010@sjtu.edu.cn

[†]jliu@phy.duke.edu

[‡]yijia_tang@sjtu.edu.cn

Various numerical methods have been proposed for the PB equation in literature [31], such as the finite difference method (FD) [11, 6, 17], finite element method (FEM) [7, 2, 5] and boundary element/integral method [3, 30].

In this work, we seek a direct particle method to simulate the motion of ionic particles in solution instead of solving the mean-field PNP equation and its steady state PB equation. The advantages are two-sided. On the one hand, particle simulation can render the transient phenomena, though in this work our main focus is the stationary problem and the equilibriums. On the other hand, particle method is insensitive to dimensionality and geometry. The aforementioned FD or FEM methods are feasible for solving the nonlinear PB equation in 1D and 2D with some simple geometry of the membrane or molecular surface, but they are not very convenient for complex geometry or in high dimensions. For example, particle method is preferable in modeling the dynamics of protein folding in mobile ionic water solvent despite of complex protein structure. In this work, the finite size of ions, ion channels, collision and non-Coulombic interaction are ignored, which can be taken into account in the generalized PB equation. Particle simulations of these physical features are left to future work.

In our particle simulation, each particle will interact with the others through the long range Coulomb interaction. To reduce the computational cost, we adopt the Random Batch Method for interacting particle systems proposed by Jin et al in [20]. This method utilizes small but random batch idea so that interactions only occur inside the small batches. For a system of N particles, it reduces the computational cost per time step from $\mathcal{O}(N^2)$ to $\mathcal{O}(N)$ in a surprisingly simple way. Another benefit of RBM is that it is not necessary to consider hard sphere potential such as Lennard-Jones potential. The RBM has been successfully applied to the Stein Variational Gradient Descent for efficient sampling from a given probability measure in [26] and to N -body quantum dynamics in [12].

Last but not least, we note that, in the original setting, the charged cell is immersed in some unbounded solution. A natural idea is to truncate the domain and prescribe a suitable boundary condition to the artificial surface. Here, we use the reflecting boundary condition and derive an approximating PB system in the truncated domain. A convergence result will be proved, which says the solution of the PB equation in truncated domain can well approximate the solution of the original problem. This means one only needs to simulate the ionic particles in a suitably truncated domain.

The rest of the paper is organized as follows. In section 2, we briefly introduce the PB equation from a microscopic point of view and some basic setup. In section 3, we present an approximating model by truncating the domain. In section 4, we explain the details of the direct simulation approach to the PB equation in a truncated domain using RBM and address several issues in implementation. In section 5, we obtain an error estimate in Theorem 5.1, which demonstrates that the solution of the approximating PB equation converges exponentially to the solution of the original PB equation in some special cases. Numerical tests are given in section 6, which show that our method can well capture the screening layer. Concluding remarks are drawn in section 7.

2 The Poisson-Boltzmann equation

In this section, we first give a brief derivation of the Poisson-Boltzmann equation starting from the Langevin equation describing the motion of microscopic particle. Then we perform nondimensionalization for the PB equation.

2.1 The mathematical setup

Consider a cell $\mathcal{C} \subset \mathbb{R}^d$ with some free charges in it. Put the cell in some electrolyte solution Ω with J ionic species. In this setup, $\mathcal{C} = \bar{\Omega}^c$. We assume the dielectric constant of the solvent does not change too much from inside to outside of \mathcal{C} , so we will assume the dielectricity ε is a constant throughout this work. See Appendix A for some discussions on the effects of different dielectricity. Let ρ_f be the distribution of charges inside the cell

which we regard as unchanged during the whole process. Denote the membrane of the cell as $\Gamma = \partial\mathcal{C}$. We will also assume the membrane has a fixed shape and the ions can not go through the membrane since we do not consider ion channels here. Then the ions will concentrate close to the membrane and form a screening layer in several Debye lengths [1].

In this work, the finite size of the ions outside the cell is considered negligible, so the ions can be treated as point charges. For a typical ionic particle X_j of the j -th species ($1 \leq j \leq J$) with valence z_j , it is subject to the electric field and collision with molecules of the solvent. The collision with molecules is modeled by friction and white noise. Note that we assume the electrolyte is dilute so that the collision effect and non-Coulombic interactions between ions are ignored. Then the motion of X_j is described by the overdamped Langevin system

$$dX_j = -\frac{1}{\gamma} \nabla(z_j e \Phi) dt + \sqrt{2D} dB + dR. \quad (2.1)$$

Here dX_j comes from the friction term so that $X_j \in \mathbb{R}^d$ is the location of the particle. e is the electron charge, Φ is the total electronic potential, $-z_j e \nabla \Phi$ represents the electronic force. D is the diffusion constant satisfying Einstein relation $D = k_B T / \gamma$, where k_B , T and γ denote the Boltzmann constant, the absolute temperature and the viscosity coefficient respectively. Note that here $[B] = \sqrt{[t]}$, where $[\cdot]$ represents the dimension, (the scale of time $[t]$ is chosen as $\frac{L_c^2}{D}$ in the next subsection), this gives $B(t) = \sqrt{[t]} \tilde{B}\left(\frac{t}{[t]}\right)$ with $\tilde{B}(\cdot)$ being a standard Brownian motion. Furthermore, $R(t) \in \mathbb{R}^d$ is the reflecting process associated to X_j which prohibits X_j from crossing the membrane. Then $X_j(t)$ is a Ω -valued process and $R(t)$ satisfies

$$R(t) = \int_0^t \mathbf{n}(X_j) d|R|_s, \quad |R|_t = \int_0^t \mathbb{1}_\Gamma(X_j) d|R|_s. \quad (2.2)$$

Here, $\mathbf{n}(X_j)$ denotes the outward unit normal to Γ at the point $X_j \in \Gamma$, $R(0) = 0$, and $|R|_t$ is the total variation of $R(t)$ on $[0, t]$, namely,

$$|R|_t = \sup \sum_{k=1}^n |R(t_k) - R(t_{k-1})|,$$

where the supremum is taken over all partitions $0 \leq t_0 < t_1 < \dots < t_n = t$.

The reflecting stochastic differential equation (RSDE) (2.1)-(2.2) is also called Skorokhod SDE. Finding the solution pair (X_j, R) to the RSDE is the well-known Skorokhod problem, which was pioneered by Skorokhod in [38, 39], where the reflecting process in a half line $[0, \infty)$ was taken into account. Later on, Tanaka [41] considered the multi-dimensional case in a convex domain. Lions and Sznitman [27] considered more general domain satisfying the admissibility condition, and the admissibility condition has been removed in [36] by Saisho. At the discrete level, RSDE can be solved by some standard numerical methods [32, 34, 40, 42], which combines the widely used Euler-Maruyama scheme and some reflecting techniques, such as penalization, projection and reflection.

Let ρ_j be the macroscopic species density of the j -th species outside the cell. By Itô's formula, ρ_j corresponding to systems (2.1)-(2.2) is governed by the Nernst-Planck equation (see section 3.1 in [35] for similar formal derivation)

$$\begin{cases} \partial_t \rho_j = \nabla \cdot \left(\frac{1}{\gamma} \nabla(z_j e \Phi) \rho_j \right) + \Delta(D \rho_j), & x \in \Omega, t > 0, \\ \rho_j|_{t=0} = \rho_{0,j}, & x \in \Omega, \\ \left\langle \frac{1}{\gamma} \nabla(z_j e \Phi) \rho_j + \nabla(D \rho_j), \mathbf{n} \right\rangle = 0, & x \in \Gamma, \end{cases} \quad (2.3)$$

coupled with the Poisson equation for the total electronic potential Φ

$$-\varepsilon \Delta \Phi = e \sum_{j=1}^J z_j \rho_j, \quad x \in \Omega, \quad (2.4)$$

where $\varepsilon = \varepsilon_0 \varepsilon_r$ is the dielectric constant of the solvent, \mathbf{n} is the unit exterior normal of Γ (pointing to Ω). Denote σ_f as the equivalent effective surface charge for inside charges ρ_f . This means σ_f gives exactly the same field as ρ_f for $x \in \Omega$ and

$$e \int_{\mathcal{C}} \rho_f dx = \oint_{\Gamma} \sigma_f dS_x.$$

Note that we have assumed the dielectric constants are the same inside and outside the cell. From Gauss's law, it holds

$$-\varepsilon \nabla \Phi \cdot \mathbf{n} \big|_{\Gamma} = \sigma_f, \quad (2.5)$$

which gives the boundary condition for the external Poisson equation. The coupling of the Nernst-Planck equation and the Poisson equation is the well-known PNP system.

For the Nernst-Planck equation (2.3), the stationary distribution has the form of

$$\rho_j = c_j \exp \left(-\frac{z_j e \Phi}{k_B T} \right)$$

with c_j a positive constant. Provided the system satisfies the electroneutrality condition

$$\sum_{j=1}^J z_j \rho_j^\infty = 0,$$

where ρ_j^∞ is the far field concentration, one has $\Phi(x) \rightarrow 0$ as $|x| \rightarrow \infty$ and thereby $c_j = \rho_j^\infty$. Hence, the stationary species density is given by the Boltzmann distribution

$$\rho_j = \rho_j^\infty \exp \left(-\frac{z_j e \Phi}{k_B T} \right), \quad j = 1, \dots, J. \quad (2.6)$$

Consequently, the steady state Poisson equation becomes

$$\begin{cases} -\varepsilon \Delta \Phi = e \sum_{j=1}^J z_j \rho_j^\infty \exp \left(-\frac{z_j e \Phi}{k_B T} \right), & x \in \Omega, \\ -\varepsilon \nabla \Phi \cdot \mathbf{n} = \sigma_f, & x \in \Gamma, \quad \Phi(x) \rightarrow 0 \text{ as } |x| \rightarrow \infty. \end{cases} \quad (2.7)$$

This is the so-called Poisson-Boltzmann equation. Notice that σ_f is a given function in (2.5) totally determined by the free charge distribution ρ_f .

2.2 Nondimensionalization

Denote L_c as the diameter of the cell \mathcal{C} and ρ_c as the characteristic concentration. Introduce the Debye length defined by $\lambda_D = \sqrt{\frac{\varepsilon k_B T}{e^2 \rho_c}}$ and a parameter $\nu = \left(\frac{\lambda_D}{L_c} \right)^2$. Then, one can rescale the variables

$$\tilde{x} = \frac{x}{L_c}, \quad \tilde{t} = \frac{Dt}{L_c^2}$$

and introduce the following dimensionless quantities

$$\tilde{\Phi} = \frac{e \Phi}{k_B T}, \quad \tilde{\sigma}_f = \frac{e L_c \sigma_f}{\varepsilon k_B T}, \quad \tilde{\rho}_j = \frac{\rho_j}{\rho_c}, \quad \tilde{\rho}_j^\infty = \frac{\rho_j^\infty}{\rho_c}, \quad \tilde{\rho}_f = \frac{\rho_f}{\rho_c}, \quad \tilde{\rho}_{0,j} = \frac{\rho_{0,j}}{\rho_c}.$$

Let $\tilde{\mathcal{C}} = \{\tilde{x} \in \mathbb{R}^d : \tilde{x} L_c \in \mathcal{C}\}$, $\tilde{\Gamma} = \partial \tilde{\mathcal{C}}$, $\tilde{\Omega} = \mathbb{R}^d \setminus \tilde{\mathcal{C}}$. For simplicity, the tildes over all quantities are dropped. With the the electroneutrality condition $\sum_{j=1}^J z_j \rho_j^\infty = 0$, the

dimensionless PNP system reads

$$\begin{cases} \partial_t \rho_j = \nabla \cdot (\nabla (z_j \Phi) \rho_j) + \Delta \rho_j, & x \in \Omega, t > 0, \\ -\nu \Delta \Phi = \sum_{j=1}^J z_j \rho_j, & x \in \Omega, \\ \langle \nabla (z_j \Phi) \rho_j + \nabla \rho_j, \mathbf{n} \rangle = 0, & x \in \Gamma, \\ \rho_j|_{t=0} = \rho_{0,j}, & x \in \Omega, \\ -\nabla \Phi \cdot \mathbf{n} = \sigma_f, & x \in \Gamma, \quad \Phi(x) \rightarrow 0 \text{ as } |x| \rightarrow \infty, \end{cases} \quad (2.8)$$

while the dimensionless PB system at equilibrium reads

$$\begin{cases} -\nu \Delta \Phi = \sum_{j=1}^J z_j \rho_j^\infty \exp(-z_j \Phi), & x \in \Omega, \\ -\nabla \Phi \cdot \mathbf{n} = \sigma_f, & x \in \Gamma, \quad \Phi(x) \rightarrow 0 \text{ as } |x| \rightarrow \infty. \end{cases} \quad (2.9)$$

Note that the surface charge density σ_f satisfies

$$\int_{\mathcal{C}} \rho_f dx = \nu \oint_{\Gamma} \sigma_f dS_x =: Q_f.$$

For simplicity, we only consider symmetric monovalent electrolyte throughout this paper, i.e. $J = 2, j = \pm, z_+ = 1, z_- = -1$. In this case, due to electroneutrality,

$$\rho_\infty := \rho_+^\infty = \rho_-^\infty.$$

Then, the nonlinear Poisson-Boltzmann system under investigation is

$$\begin{cases} -\nu \Delta \Phi = \rho_\infty (e^{-\Phi} - e^{\Phi}), & x \in \Omega, \\ -\nabla \Phi \cdot \mathbf{n} = \sigma_f, & x \in \Gamma, \quad \Phi(x) \rightarrow 0 \text{ as } |x| \rightarrow \infty. \end{cases} \quad (2.10)$$

From formal asymptotic expansion, we know there is a boundary layer (the so-called Debye screening layer) around Γ whose thickness is of $\mathcal{O}(\sqrt{\nu})$ [1]. See section 6 for numerical verification.

3 Approximating by truncated domain

In practice, it may be difficult to solve a PDE in unbounded domain. Instead of solving the mean-field PB equation (2.10) for the equilibrium, we seek a particle method that directly simulates the dynamics of the ions.

At the microscopic level, the underlying RSDE for (2.8) is given by

$$\begin{cases} dX_j = -\nabla (z_j \Phi) dt + \sqrt{2} dB + dR, \\ R(t) = \int_0^t \mathbf{n}(X_j) d|R|_s, \quad |R|_t = \int_0^t \mathbb{1}_\Gamma(X_j) d|R|_s. \end{cases} \quad (3.1)$$

This is the dimensionless version of (2.1). Again, the reflecting process R associated to X_j prevents X_j from going into \mathcal{C} .

We aim to simulate (3.1). Since $\rho_\infty \neq 0$, we have $\int_{\Omega} \rho_\pm dx = \int_{\Omega} \rho_\infty e^{\mp \Phi} dx = +\infty$, which means the total positive and negative charge are infinite in the unbounded external domain. However, we can only simulate finite number of particles in particle simulation. This motivates us to truncate the domain, as discussed below.

3.1 Reflecting stochastic differential equation with an artificial wall

Intuitively, consider, for example, NaCl solution in an unbounded container. Put a charged cell in it, a screening layer is formed immediately to neutralize the effective surface charge on the membrane, Cl^- and Na^+ away from the membrane reach a dynamic equilibrium with concentration ρ_∞ . Physically, there is a big reservoir with inexhaustible Cl^- and Na^+ . When one looks at a sphere $B_L = \{|x| < L\}$ large enough, in order to ensure the conservation of density and momentum, the influx of ions should be equivalent to the outflux of ions through ∂B_L in the sense of charges and heat. Although an ion would not change its direction at once when it crosses ∂B_L , there would be another ion from the reservoir which gets inside. Since we only care about the statistical behavior of Cl^- and Na^+ , we can simply bounce an ion back when it crosses ∂B_L as if there was a virtual wall. This motivates us to consider an approximating problem in a truncated domain and impose a reflecting boundary condition in the artificial wall. See section 5 for mathematical justification of introducing a truncated domain in PDE level for some cases.

Let $B_L = \{|x| < L\}$ be a sufficiently large ball containing the cell \mathcal{C} and $\Omega_L = B_L \setminus \bar{\mathcal{C}}$. As mentioned before, one can only simulate the motion of charged particles in the truncated domain Ω_L . Besides the reflecting process on the inner boundary Γ , we also use a reflecting boundary condition for ∂B_L . Thus the approximating RSDE with artificial wall reads

$$\begin{cases} dX_j = -\nabla(z_j \hat{\Phi}_L)dt + \sqrt{2}dB + dR, \\ R(t) = \int_0^t \mathbf{n}(X_j)d|R|_s, \quad |R|_t = \int_0^t \mathbb{1}_{\partial\Omega_L}(X_j)d|R|_s, \quad X_j(0) = X_{0,j} \sim \rho_{0,j}. \end{cases} \quad (3.2)$$

Here, the subscript L is used to emphasize the truncated domain. The physical potential $\hat{\Phi}_L$ should be determined in a consistent way in the sense that the charge density of the j -th species should be proportional to the law of X_j . Moreover, $\partial\Omega_L = \Gamma \cup \partial B_L$, the reflecting process R ensures the particle stay in Ω_L .

3.2 The approximating Poisson-Boltzmann equation with an artificial wall

At the macroscopic level, the Nernst-Planck equations in Ω_L corresponding to (3.2) are

$$\begin{cases} \partial_t \rho_j = \nabla \cdot (\nabla(z_j \hat{\Phi}_L) \rho_j) + \Delta \rho_j, & x \in \Omega_L, t > 0, \\ \langle \nabla(z_j \hat{\Phi}_L) \rho_j + \nabla \rho_j, \mathbf{n} \rangle = 0, & x \in \partial\Omega_L, \\ \rho_j|_{t=0} = \rho_{0,j}, & x \in \Omega_L. \end{cases} \quad j = \pm. \quad (3.3)$$

The boundary condition used here is the no-flux boundary condition. This ensures the total positive charge $Q_+ = \int_{\Omega_L} \rho_+ dx$ and total negative charge $Q_- = \int_{\Omega_L} \rho_- dx$ are conserved.

The total potential $\hat{\Phi}_L$ is generated by the free charges ρ_f in \mathcal{C} and the charges ρ_\pm in Ω_L . Due to the assumption of uniform dielectricity, one has

$$\hat{\Phi}_L = (\rho_f + \rho_+ - \rho_-) * \Psi. \quad (3.4)$$

Here Ψ is the Coulomb potential given by

$$\Psi(x) = \begin{cases} -\frac{1}{2\nu} |x|, & d = 1, \\ -\frac{1}{2\pi\nu} \ln |x|, & d = 2, \\ \frac{1}{d(d-2)\alpha(d)\nu|x|^{d-2}}, & d \geq 3, \end{cases} \quad (3.5)$$

where $\alpha(d) = \frac{\pi^{d/2}}{\Gamma(d/2+1)}$ denotes the volume of the unit ball in \mathbb{R}^d . Physically, since the dielectric constants are the same in Ω and \mathcal{C} , there is no induced charge on the inner boundary Γ as well as the artificial boundary ∂B_L , so Ψ is the fundamental solution to

$-\nu\Delta\Psi = \delta$ in the whole space. See Appendix A for more discussions on variable dielectric constants.

The stationary solutions to (3.3) still have the form

$$\rho_+ = C_+ e^{-\hat{\Phi}_L}, \quad \rho_- = C_- e^{\hat{\Phi}_L}.$$

Then the steady state Poisson equation reads

$$-\nu\Delta\hat{\Phi}_L = C_+ e^{-\hat{\Phi}_L} - C_- e^{\hat{\Phi}_L}, \quad x \in \Omega_L, \quad (3.6)$$

C_+, C_- are to be determined.

For the original PB equation (2.10), $\rho_+^\infty = \rho_-^\infty = \rho_\infty$. Otherwise, if the infinite concentration of positive and negative charges is not equal, the net charge of the physical system $Q_f + \int_{\Omega} \rho_+ - \rho_- dx$ is infinite since $\rho_+ \rightarrow \rho_+^\infty, \rho_- \rightarrow \rho_-^\infty$ as $|x| \rightarrow \infty$. However, in the bounded case, it is not necessary that $\rho_+ = \rho_-$ for all $x \in \partial B_L$. But we can impose

$$\rho_+(\bar{x})\rho_-(\bar{x}) = \rho_\infty^2 \quad (3.7)$$

at some point $\bar{x} \in \partial B_L$ by adjusting the total charge of positive ions. For example, in 1D, we can require $\rho_+(L)\rho_-(L) = \rho_\infty^2$. While in 3D, we can pick a point $\bar{x} = (L, 0, 0)$ such that $\rho_+(\bar{x})\rho_-(\bar{x}) = \rho_\infty^2$. Thus, $C_+C_- = \rho_\infty^2$, and there exists a constant c such that

$$C_+ = \rho_\infty e^{-c}, \quad C_- = \rho_\infty e^c. \quad (3.8)$$

There is no doubt that the boundary condition on Γ is

$$-\frac{\partial\hat{\Phi}_L}{\partial\mathbf{n}}\Big|_\Gamma = \sigma_f. \quad (3.9)$$

The remaining problem is to prescribe a suitable boundary condition on ∂B_L . For potential (3.4), the physical boundary condition to particle simulation with reflection at ∂B_L is

$$\frac{\partial\hat{\Phi}_L}{\partial\mathbf{n}}\Big|_{\partial B_L} = \mathbf{n} \cdot \nabla [(\rho_f + \rho_+ - \rho_-) * \Psi]. \quad (3.10)$$

We also remark that $\int_{\partial B_L} \frac{\partial\hat{\Phi}_L}{\partial\mathbf{n}} dS_x = 0$ due to zero net charge at ∂B_L .

Let $\Phi_L = \hat{\Phi}_L + c$. Combing (3.6)-(3.10) yields

$$\begin{cases} -\nu\Delta\Phi_L = \rho_\infty (e^{-\Phi_L} - e^{\Phi_L}), & x \in \Omega_L, \\ -\frac{\partial\Phi_L}{\partial\mathbf{n}}\Big|_\Gamma = \sigma_f, \quad \frac{\partial\Phi_L}{\partial\mathbf{n}}\Big|_{\partial B_L} = \mathbf{n} \cdot \nabla [(\rho_f + \rho_\infty e^{-\Phi_L} - \rho_\infty e^{\Phi_L}) * \Psi], \end{cases} \quad (3.11)$$

which is the approximating PB equation in the truncated domain.

4 The Random Batch particle system for the Poisson-Boltzmann equation

In (3.2), $\hat{\Phi}_L$ is generated by the free charges and continuous distributions of positive and negative charges as (3.4) shows. The law of positive or negative charge is proportional to ρ_+ or ρ_- . Hence, (3.2) can be regarded as the mean field limit of interacting particle systems. To numerically simulate (3.2), we simulate N particles that interact with each other through Coulomb interaction, hoping that the empirical measure of positive particles ρ_+^N multiplied by total positive charge Q_+ is the approximation to ρ_+ , and the same argument holds for ρ_- . That is,

$$\rho_+^N = \frac{1}{N_+} \sum_{i \in I_+} \delta(\cdot - X^i), \quad \rho_-^N = \frac{1}{N_-} \sum_{i \in I_-} \delta(\cdot - X^i),$$

and in the $N \rightarrow \infty$ regime,

$$Q_+\rho_+^N \rightharpoonup \rho_+, \quad Q_-\rho_-^N \rightharpoonup \rho_-.$$

Here, the superscript i denotes the i -th particle, $I_+ = \{i, z^i = 1\}$, $I_- = \{i, z^i = -1\}$ with z^i being the sign of X^i . N_+, N_- are the number of positive and negative charges. The total particle number is $N = N_+ + N_-$.

4.1 Interacting particle systems

Let

$$F = -\nabla \Psi, \quad E_f = \rho_f * F,$$

so that F is the Coulomb repulsive force and E_f is the electronic field generated by ρ_f . Then, the above interpretation implies that we can approximate the self-consistent RSDE (3.2) through the interacting particle systems

$$\begin{cases} dX^i = z^i E_f(X^i)dt + \sum_{k:k \neq i} z^i z^k \frac{|Q|}{N} F(X^i - X^k)dt + \sqrt{2}dB^i + dR^i, & i = 1, \dots, N, \\ R^i(t) = \int_0^t \mathbf{n}(X^i)d|R^i|_s, \quad |R^i|_t = \int_0^t \mathbf{1}_{\partial\Omega_L}(X^i)d|R^i|_s, \quad X^i(0) = X_0^i. \end{cases} \quad (4.1)$$

Here $\{X^i\}_{i=1}^N$ are the trajectories of N particles and the particles from all species are numbered together. $\{B^i\}_{i=1}^N$ are N independent d -dimensional Brownian motions and $\{R^i\}_{i=1}^N$ are reflecting processes associated to $\{X^i\}_{i=1}^N$. The initial data $\{X_0^i\}_{i \in I_{\pm}}$ are independent, identically distributed (i.i.d.) random variables with probability density function $\rho_{0,\pm}$. $|Q| = Q_+ + Q_-$ is total absolute charge in Ω_L (not to be confused with total net charge $Q_+ - Q_-$ in Ω_L). Let $q = \frac{|Q|}{N}$. Then each particle has charge $\pm q$. $N_+ = \frac{Q_+}{q}$, $N_- = \frac{Q_-}{q}$. Note that the 'particle' here can be either 'numerical particle' or 'physical particle'.

Remark 4.1. For interacting particle system (4.1), there is some probability that two opposite particles attract each other. When a positive and a negative charge meet, they cancel each other and there is energy jump (the interaction energy is frozen and set to zero). In the $N \rightarrow \infty$ limit, each particle carries infinitely small charge and this cancellation will not affect the continuum interaction energy. However, for the finite N particle systems, once two opposite particles meet, the attraction force between them is infinite. Thus, they stick together and it is impossible to set them apart in subsequent steps. Hence, one needs to add some hard sphere potential to avoid this unphysical attraction and cancellation. What people usually do is to introduce the Lennard-Jones potential [22, 25].

Direct simulation of (4.1) is expensive due to the nonlocal interaction term. Solving it requires $\mathcal{O}(N^2)$ operation per time step, so we apply Random Batch Method in [20] to reduce computational cost to $\mathcal{O}(N)$ per time step. Below, we briefly introduce Random Batch Method in section 4.2, then apply it to systems (4.1) in section 4.3 and address some implementation issues in section 4.4.

4.2 A brief introduction to the Random Batch Method

To improve computational efficiency for binary interacting particle systems

$$dX^i = -\nabla V(X^i)dt + \frac{1}{N-1} \sum_{k:k \neq i} F(X^i - X^k)dt + \sigma dB^i, \quad i = 1, \dots, N. \quad (4.2)$$

Jin, Li and Liu [20] proposed the Random Batch Method. The idea is to randomly divide the N particles into n small batches with batch size p ($p \ll N$) and interact them within each batch for each time step. That is, to solve the following SDE

$$dX^i = -\nabla V(X^i)dt + \frac{1}{p-1} \sum_{k \in \mathcal{C}_q, k \neq i} F(X^i - X^k)dt + \sigma dB^i, \quad i \in \mathcal{C}_q \quad (4.3)$$

for each time interval $[t_{m-1}, t_m]$. Here, the discrete time $t_m = m\tau$, where τ is the time step. \mathcal{C}_q , $q = 1, \dots, n$ denote the random batches, which will be renewed at each time grid points. Thus, the computational cost is reduced from $\mathcal{O}(N^2)$ to $\mathcal{O}(pN)$ per time step.

The main theoretical results are the following error estimates

Proposition 4.2 ([20, Theorem 3.1]). *Suppose the confining potential V is strongly convex and the interacting force F is bounded and Lipschitz,*

$$\sup_{t \geq 0} \|X^1(t) - \tilde{X}^1(t)\| = \sup_{t \geq 0} \sqrt{\mathbb{E} |X^1(t) - \tilde{X}^1(t)|^2} \leq C \sqrt{\frac{\tau}{p-1} + \tau^2}, \quad (4.4)$$

where C is independent of N, p . Here X^1 denotes the solution of N particle systems (4.2) while \tilde{X}^1 denotes the solution of RBM (4.3) under the same Brownian motion and the same initial distribution. Consequently, Let $\mu_N^{(1)}(t)$ and $\tilde{\mu}_N^{(1)}(t)$ be the first marginal for (4.2) and (4.3) respectively. Then

$$\sup_{t \geq 0} W_2(\mu_N^{(1)}(t), \tilde{\mu}_N^{(1)}(t)) \leq C \sqrt{\frac{\tau}{p-1} + \tau^2} \leq C\sqrt{\tau}. \quad (4.5)$$

Estimate (4.4) says that RBM can approximate the trajectories of particles in strong sense, while (4.5) tells that the distribution for RBM is close to the distribution generated by full particle systems under Wasserstein distance with convergence rate $\mathcal{O}(\sqrt{\tau})$. Moreover, the next result says RBM can capture the solution $\mu(t)$ of the mean field equation

$$\partial_t \mu = \nabla \cdot (\nabla V(x)\mu) - \nabla \cdot (\mu F * \mu) + \frac{1}{2} \sigma^2 \Delta \mu \quad (4.6)$$

in the $N \rightarrow +\infty$ regime.

Proposition 4.3 ([20, Corollary 3.1]). *Under the same assumptions,*

$$W_2(\mu(t), \tilde{\mu}_N^{(1)}(t)) \leq C(\sqrt{\tau} + N^{-\frac{1}{2}+\varepsilon}). \quad (4.7)$$

Since the error bound is uniform in time, the limits $N \rightarrow +\infty$ and $t \rightarrow +\infty$ commute. Therefore, RBM can well approximate the invariant measure π of (4.6). Since the charge density distributions of the PB equation are the invariant measure of PNP systems. By Proposition 4.3, we expect that RBM can compute solution to PB approximately.

4.3 The Random Batch Method for the PB equation (RBM-PB)

In this work, we apply RBM to simulate systems (4.1). Motivated by Proposition 4.3, we expect that RBM can approximate solutions to PB equation. We note, however, that the theories in [20] do not apply directly to (4.1). The interacting particle systems here involve particles that are not identical, while the original RBM method in [20] was for indistinguishable particles. Recently, Jin, Li and Liu [19] extend the convergence results of RBM for interacting particles with disparate species and weights. Note that the Coulomb interacting force is singular for $d \geq 2$, this does not satisfy the condition in Proposition 4.2. However, simulation results in section 6 indicate that the numerics can go far beyond the theory as pointed out in [20].

The corresponding RBM system reads: $t \in [t_{m-1}, t_m]$, for $q = 1, \dots, n$,

$$\left\{ \begin{array}{l} dX^i = z^i E_f(X^i) dt + \frac{1}{p-1} \sum_{k \in \mathcal{C}_q: k \neq i} z^i z^k |Q| \frac{N-1}{N} F(X^i - X^k) dt \\ \quad + \sqrt{2} dB^i + dR^i, \quad i \in \mathcal{C}_q, \\ R^i(t) = \int_0^t \mathbf{n}(X^i) d|R^i|_s, \quad |R^i|_t = \int_0^t \mathbb{1}_{\partial\Omega_L}(X^i) d|R^i|_s, \quad X^i(0) = X_0^i. \end{array} \right. \quad (4.8)$$

We call this interacting particle systems RBM-PB. Therefore, by simulating systems (4.8), we expect to obtain the desired equilibrium distributions for PB equation (3.11).

Unlike the full particle systems (4.1), for RBM-PB systems (4.8), there is no need to consider hard sphere potential since we do random reshuffling before each time step. If two opposite particles encounter (they are in the same batch and the distance between them is zero) at a certain time step, it is of high probability that they get lost (they are in different batches) in the next time step. Owing to the random mini batch idea, two particles being stuck all the time is an impossible event, which do not have to be taken care of.

Once we have obtained the equilibrium distributions ρ_+ and ρ_- by simulation, there are two approaches to computing potential Φ_L . On the one hand, we can take logarithm directly since $\Phi_L = \ln \frac{\rho_\infty}{\rho_+} = \ln \frac{\rho_-}{\rho_\infty}$. On the other hand, we can solve $-\nu \Delta \Phi_L = \rho_+ - \rho_-$ by some fast Poisson solver such as fast cosine transform [37]. This is quite efficient compared to solving the nonlinear PB equation.

4.4 Some implementation issues about RBM-PB

In this subsection, we make some discussions about RBM-PB in implementations. The first issue is how to impose condition (3.7) in simulation, the second issue deals with the singular interacting force F in (4.8) when $X^i \approx X^k$ for $d \geq 2$.

4.4.1 An iterative method for Q_+ with fixed ρ_∞

In simulation of RBM-PB (4.8), the total positive or negative charge Q_\pm is assumed to be known. However, in practical problems, what we often know is the infinite concentration ρ_∞ . Because we can get the ionic concentrations of the solution through measurements. Namely, we care about the case where ρ_∞ is given instead of Q_+ .

One can see from Figure 1 that: with fixed Q_f , the larger Q_+ is, the larger ρ_∞ will be. Though plotted in 1D, it holds for higher dimensions. Since each particle shares charge q , larger Q_+ represents more positive particles. So we can run the particle simulation by iteration without a prior knowledge of the total positive charge Q_+ and adjust the particles adaptively.

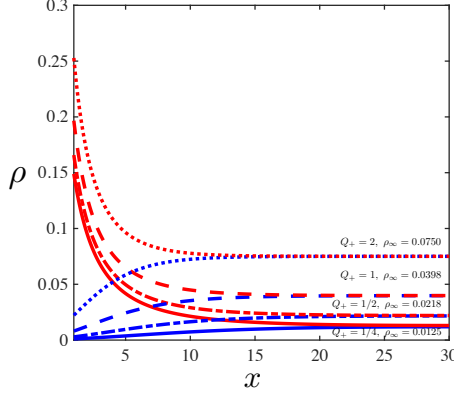


Figure 1: The equilibrium distributions (red for ρ_- , blue for ρ_+) in 1D with fixed $Q_f = 1$. The truncated domain is $[1, 10]$. This shows ρ_∞ is larger when Q_+ is larger.

Based on this observation, we design an iterative algorithm to determine Q_+ with fixed ρ_∞ . In each iteration, first run RBM-PB simulation for an empirical time T_c to reach the equilibrium state (i.e. when the empirical density distributions do not change anymore) for the initial guess of Q_+ . Then compute the densities $\rho_\pm(\bar{x})$ at some fixed point $\bar{x} \in \partial B_L$. If $\rho_+(\bar{x})\rho_-(\bar{x})$ is lower than ρ_∞^2 , randomly add some positive and negative particles into the ensemble. Otherwise, randomly kill some positive and negative particles. Since $Q_- = Q_+ + Q_f$, the change of positive and negative particles should be the same to maintain the total net charge in Ω_L . The iteration terminates when condition (3.7) is satisfied within

tolerance. After iteration, one can get the true Q_+ . The process is illustrated in Algorithm 1.

Algorithm 1 Iterative method for Q_+ with fixed ρ_∞

Input Initial distributions $\rho_{0,\pm}$, truncated length L , total surface charge Q_f , charge per particle q , infinite concentration ρ_∞ , a point $\bar{x} \in \partial B_L$, empirical time T_c , tolerance ϵ .

```

1: Initial guess  $Q_+$ ,  $Err = 1$ .
2: Generate  $N_+ = \frac{Q_+}{q}$  samples from  $\rho_{0,+}$  and  $N_- = \frac{Q_-}{q} = \frac{Q_+ + Q_f}{q}$  samples from  $\rho_{0,-}$ .
3: while  $Err > \epsilon$  do
4:   Run particle simulation for  $T_c$  by RBM-PB.
5:   Calculate the densities  $\rho_\pm(\bar{x})$ .
6:    $I = \rho_+(\bar{x})\rho_-(\bar{x}) - \rho_\infty^2$ , error  $Err = \sqrt{I}$ , the approximate charge change  $\Delta Q := \frac{\alpha(d)L^d}{2}Err$ . Then  $\Delta N := \left\lfloor \frac{\Delta Q}{q} \right\rfloor$ ,  $\Delta Q' = q\Delta N$ .
7:   if  $Err < 0$  then
8:     Generate  $\Delta N$  samples from  $\rho_{0,\pm}$  and add them to the positive particles and the negative particles respectively. Set  $Q_+ \leftarrow Q_+ + \Delta Q'$ .
9:   else
10:    Remove  $\Delta N$  samples from the positive particles and negative particles respectively. Set  $Q_+ \leftarrow Q_+ - \Delta Q'$ .
11:   end if
12: end while

```

Output $Q_+, \rho_+, \rho_-, \Phi_L$.

In Algorithm 1, the bulk densities $\rho_\pm(\bar{x})$ are

$$\rho_\pm(\bar{x}) = \frac{2N_\pm(D_h)}{\alpha(d)h^d N_\pm},$$

where D_h is a small half ball $\{x \in \Omega_L : |x - \bar{x}| \leq h\}$ around \bar{x} , $N_\pm(D_h)$ are the number of positive or negative particles in D_h . Due to random fluctuation, the calculation of bulk densities is not stable, thus the iteration may not converge. A direct way to avoid random fluctuation is to increase particle number, but this is expensive. Another widely used approach is time average, which is the average of densities of previous iterations after reaching equilibrium.

4.4.2 A splitting strategy for RBM-PB in high dimension ($d \geq 2$)

The Coulomb repulsive force is $F(x) = -\nabla\Psi = \frac{x}{d\alpha(d)\nu|x|^d}$ in d dimension. Note that F is singular when $d \geq 2$, so we adopt the splitting strategy mentioned in [20] to solve RBM-PB. (4.8) can be split into

$$\begin{cases} dX^i = \frac{1}{p-1} \sum_{k \in \mathcal{C}_q: k \neq i} z^i z^k |Q| \frac{N-1}{N} F(X^i - X^k) dt, \\ dX^i = z^i E_f(X^i) dt + \sqrt{2} dB^i + dR^i. \end{cases}$$

Thus we can solve the first equation analytically when $p = 2$. In particular, for i, k in the same batch, defining

$$v = \frac{X^i(0) - X^k(0)}{|X^i(0) - X^k(0)|}, \quad \beta = \frac{2z^i z^k |Q|(N-1)}{\alpha(d)\nu N},$$

one has

$$\begin{aligned} X^i(t) &= \frac{1}{2} \left\{ (X^i(0) + X^k(0)) + v \left(\left| X^i(0) - X^k(0) \right|^d + \beta t \right)^{1/d} \right\}, \\ X^k(t) &= \frac{1}{2} \left\{ (X^i(0) + X^k(0)) - v \left(\left| X^i(0) - X^k(0) \right|^d + \beta t \right)^{1/d} \right\}, \end{aligned}$$

under the condition $|X^i(0) - X^k(0)|^d + \beta t \geq 0$. Otherwise, let

$$X^i(t) = X^k(t) = \frac{1}{2} (X^i(0) + X^k(0)).$$

Therefore, for each time step, we exactly solve the first equation and then apply stochastic schemes to the second RSDE.

5 Error estimate for the approximating problem

In the previous section, we introduced a particle system to find the solution to the equilibrium PB equation by RBM in a bounded truncated domain. In this section, we will show in the PDE level the validity of the truncation in a special case. In other words, the solution of the PB equation in truncated domain Ω_L converges to the solution of the PB equation in Ω exponentially fast.

If ρ_f is radially symmetric, zero electronic flux in Ω_L implies the electronic field is tangential. That is to say, $\int_{\partial B_L} \frac{\partial \Phi_L}{\partial \mathbf{n}} dS_x = 0$ will reduce to $\frac{\partial \Phi_L}{\partial \mathbf{n}}|_{\partial B_L} = 0$ in this case. For simplicity, we use this homogeneous Neumann condition as the outer boundary condition for the approximating potential Φ_L for the sake of analysis. By the way, in 1D, the constraint on ρ_f can be removed due to the symmetry of electronic field $F = \frac{1}{2\nu} \operatorname{sgn}(x)$.

Without loss of generality, we assume the parameter $\nu = 1$ in this section. Consider the nonlinear Poisson-Boltzmann system

$$\begin{cases} -\Delta \Phi = \rho_\infty (e^{-\Phi} - e^\Phi), & x \in \Omega, \\ -\frac{\partial \Phi}{\partial \mathbf{n}}|_\Gamma = \sigma_f, & \Phi(x) \rightarrow 0 \text{ as } |x| \rightarrow \infty, \end{cases} \quad (5.1)$$

and the approximating problem in $\Omega_L = B_L \setminus \bar{\mathcal{C}}$

$$\begin{cases} -\Delta \Phi_L = \rho_\infty (e^{-\Phi_L} - e^{\Phi_L}), & x \in \Omega_L, \\ -\frac{\partial \Phi_L}{\partial \mathbf{n}}|_\Gamma = \sigma_f, & \frac{\partial \Phi_L}{\partial \mathbf{n}}|_{\partial B_L} = 0. \end{cases} \quad (5.2)$$

The well-posedness of (5.2) is guaranteed by classical elliptic theory [29].

Next, we will show (5.2) is a good approximation to (5.1) when the ball B_L is large enough. Approximating result here focuses on 1D and 3D. However, we believe similar convergence rate holds in other dimensions due to the exponential decay of $\nabla \Phi$. This can be estimated by analyzing the Green function of the linearized equation by boundary integral method [15, 21] like 3D.

Theorem 5.1 (Convergence). ($d = 1 \& 3$). *Let Φ be the solution of (5.1) and Φ_L that of (5.2). Then there exist constants $C_1 > 0, C_2 > 0$ independent of L such that*

$$\|\Phi_L - \Phi\|_{L^1(\Omega_L)} \leq C_2 e^{-C_1 L}$$

for L large enough.

In order to show this, we need the exponentially decay property of the solution to (5.1).

Proposition 5.2 (Exponential decay of $\Phi, \nabla \Phi$). ($d = 1 \& 3$). *There exists a positive constant R and generic constants C such that, for all $|x| > R$, the following estimates hold:*

- $d = 1$.

$$|\Phi(x)| \leq \frac{|\sigma_f|}{\sqrt{2\rho_\infty}} e^{-\sqrt{2\rho_\infty} \operatorname{dist}(x, \Gamma)},$$

$$|\Phi'(x)| \leq |\sigma_f| e^{-\sqrt{2\rho_\infty} \operatorname{dist}(x, \Gamma)}.$$

- $d = 3$.

$$|\Phi(x)| \leq \frac{C}{|x|} e^{-C|x|},$$

$$|\nabla \Phi(x)| \leq \frac{C}{|x|^2} e^{-C|x|}.$$

This proposition is proved by comparing it to a linear equation, whose solution is given by the boundary integral representation formula. So we need the following preparations: Lemma 5.3 and Lemma 5.4. The proof of Proposition 5.2 in 3D is left to Appendix B. For 1D, it is quite similar and simpler, so we omit.

Lemma 5.3 ([21] Representation formula). *If u is smooth in $\mathbb{R}^d \setminus \Gamma$ and satisfies*

$$\begin{cases} -\Delta u + cu = f & \text{in } \Omega, \\ -\Delta u + cu = 0 & \text{in } \mathcal{C}, \\ \lim_{|x| \rightarrow \infty} u = 0, \quad \lim_{|x| \rightarrow \infty} |\nabla u| = 0. \end{cases}$$

Then

$$\begin{aligned} & \int_{\Gamma} \left\{ \left[\frac{\partial u}{\partial \mathbf{n}} \right] G(x-y) - [u] \frac{\partial G(x-y)}{\partial \mathbf{n}_y} \right\} dS_y + \int_{\Omega} G(x-y) f(y) dy \\ &= \begin{cases} u(x), & x \notin \Gamma, \\ \frac{u^i(x) + u^e(x)}{2}, & x \in \Gamma. \end{cases} \end{aligned} \tag{5.3}$$

Here, G is the Green function which is the solution to $(cI - \Delta)G = \delta$. For $x \in \Gamma$, $u^i(x)$ and $u^e(x)$ represent the limit from \mathcal{C} and Ω , respectively. $[u] = u^i - u^e$.

The proof is similar to that in [21] and we omit the details.

Lemma 5.4 ([9] Comparison principle on unbounded domain). *Let $u \in C^2(\Omega) \cap C(\bar{\Omega})$. Consider an elliptic operator \mathcal{L} having the form*

$$\mathcal{L}u = -\Delta u + c(u)u,$$

where $c > 0$ is continuous. Then

$$\begin{cases} \mathcal{L}u \leq 0, & \text{in } \Omega, \\ -\frac{\partial u}{\partial \mathbf{n}} \leq 0, & \text{on } \Gamma, \quad \Rightarrow \quad u \leq 0. \\ \lim_{|x| \rightarrow \infty} u(x) = 0. \end{cases}$$

We also sketch a short proof of Lemma 5.4 in Appendix B.

Now, we are ready to prove the convergence result: Theorem 5.1. We only give a 3D proof, the 1D case can be shown without the bridge of sup solution.

Proof of Theorem 5.1 in 3D. Construct a sup solution Φ^+ which satisfies

$$\begin{cases} -\Delta \Phi^+ = \rho_{\infty} (e^{-\Phi^+} - e^{\Phi^+}), & x \in \Omega_L, \\ -\frac{\partial \Phi^+}{\partial \mathbf{n}} \Big|_{\Gamma} = \sigma_f, \quad \frac{\partial \Phi^+}{\partial \mathbf{n}} \Big|_{\partial B_L} = \Sigma_L, \end{cases} \tag{5.4}$$

where $\Sigma_L = \left\| \frac{\partial \Phi^+}{\partial \mathbf{n}} \right\|_{L^{\infty}(\partial B_L)} < +\infty$.

Let $u_1 = \Phi^+ - \Phi_L$. According to (5.4) and (5.2), u_1 satisfies

$$\begin{cases} -\Delta u_1 + cu_1 = 0, & x \in \Omega_L, \\ -\frac{\partial u_1}{\partial \mathbf{n}} \Big|_{\Gamma} = 0, \quad \frac{\partial u_1}{\partial \mathbf{n}} \Big|_{\partial B_L} = \Sigma_L, \end{cases} \quad (5.5)$$

with $c = \frac{2\rho_\infty (\sinh \Phi^+ - \sinh \Phi_L)}{\Phi^+ - \Phi_L} = 2\rho_\infty \cosh \Phi_{\xi_{u_1}} \geq 2\rho_\infty$ bounded below on Ω_L . Then by the maximum principle, we obtain

$$u_1 \geq 0. \quad (5.6)$$

Integrating equation (5.5) on Ω_L yields

$$\int_{\partial B_L} \Sigma_L dS_x = \int_{\partial \Omega_L} \frac{\partial u_1}{\partial \mathbf{n}} dS_x = \int_{\Omega_L} cu_1 dx.$$

It follows from the non-negativity of u_1 that

$$\|u_1\|_{L^1(\Omega_L)} = \left| \int_{\Omega_L} u_1 dx \right| \leq \frac{2\pi L^2}{\rho_\infty} \Sigma_L.$$

That is,

$$\|\Phi^+ - \Phi_L\|_{L^1(\Omega_L)} \leq \frac{2\pi L^2}{\rho_\infty} \|\nabla \Phi \cdot \mathbf{n}\|_{L^\infty(\partial B_L)} \leq \frac{2\pi L^2}{\rho_\infty} \|\nabla \Phi\|_{L^\infty(\partial B_L)}.$$

Similarly, let $u_2 = \Phi^+ - \Phi$ for $x \in \bar{\Omega}_L$. Then,

$$\|\Phi^+ - \Phi\|_{L^1(\Omega_L)} \leq \frac{4\pi L^2}{\rho_\infty} \|\nabla \Phi\|_{L^\infty(\partial B_L)}.$$

Hence, one concludes from Proposition 5.2 that there exist positive constants R and C_1, C_2 such that for $L > R$,

$$\|\Phi_L - \Phi\|_{L^1(\Omega_L)} \leq C_2 e^{-C_1 \sqrt{2\rho_\infty} L}.$$

□

Theorem 5.1 demonstrates the exponentially decay rate of L^1 error of Φ and Φ_L in truncated domain Ω_L . This verifies we only need to solve the PB system in Ω_L .

6 Numerics

In this section, we use a 1D example to test the effectiveness and convergence of RBM-PB simulation and a 3D example to show the applicability of RBM-PB to higher dimensional problems. The numerical results show that RBM works well in solving the PB equation in both cases.

6.1 A 1D test example

Consider a 1D example with cell $\mathcal{C} = [-1, 1]$. Assume the distribution inside the cell is $\rho_f = Q_f \delta(x)$, which corresponds to a fixed positive point charge at the origin, and the total free charge $Q_f \sim \mathcal{O}(\nu)$. Outside the cell, the solution is symmetric 1:1 salt. In order to sample from the equilibrium distributions $\rho_+ = \rho_\infty e^{-\Phi}$, $\rho_- = \rho_\infty e^{\Phi}$, we only need to simulate the particles in the bounded area $\Omega_L = (-L, -1) \cup (1, L)$ for L large enough as mentioned before. Moreover, due to symmetry, we focus on the positive half $(1, L)$ and thus consider the problem

$$\begin{cases} -\nu \Phi_L'' = \rho_\infty (e^{-\Phi_L} - e^{\Phi_L}), & 1 < x < L, \\ -\Phi_L'(1) = \sigma_f, \quad \Phi_L'(L) = 0. \end{cases} \quad (6.1)$$

where $\sigma_f = \frac{1}{2\nu} Q_f \sim \mathcal{O}(1)$ is the effective surface charge for the right half domain. Notice that $-\Phi'_L(1)$ is not $E_f(1)$ in (4.8). In 1D, the Coulomb repulsive force is $F(x) = \frac{1}{2\nu} \text{sgn}(x)$. Therefore, $E_f = \frac{1}{2\nu} \frac{Q_f}{2}$ for $x \geq 1$. However, since Φ_L is the total potential, $-\Phi'_L$ is the superposition of E_f and the field generated by ρ_+ and ρ_- , which is another $\frac{1}{2\nu} \frac{Q_f}{2}$ due to the total net charge $-\frac{Q_f}{2}$ in $(1, L)$.

As mentioned in section 2, we do not take the collision effects into consideration. This is understandable in 1D. It can be regarded as a special case in 3D, which is homogeneous in the y, z directions, only the x direction is left. So the particles can cross each other freely, or equivalently, the velocities and charges are exchanged if two of them meet.

In RBM simulation, we use three reflecting techniques to deal with the reflecting process. Denote the orthogonal projection of x on Ω_L as $\pi(x) = \arg \min_{y \in \partial\Omega_L} |x - y|$. For a particle X^i out of the truncated domain Ω_L , it is projected to the boundary by $X^i = \pi(X^i)$ in the projection scheme. In the reflection scheme, $X^i = 2\pi(X^i) - X^i$, which means finding the symmetric point inside the domain. While in the penalization scheme, it is pushed inwards to some extent by $X^i = X^i - \lambda(X^i - \pi(X^i))$, where λ is the penalty weight. We refer readers to [33, 34, 32, 40] for more details.

Next, we show the performance of RBM with three numerical reflecting methods with different scaling parameter ν . In Figure 2, $\nu = 1, Q_+ = 1, Q_f = 2\nu, N_+ = 10^5, L = 15, \tau = 0.01\nu$. The initial distributions are given by $\rho_{0,\pm} \sim \mathcal{U}[7, 8]$. We comment that the initial distributions do not affect the equilibriums. The reference solution of system (6.1) is given by Newton's iteration using FD. From Figure 2(Up), we can see that the RBM simulation results (dotted dashed lines) match well with the FD solution (black solid lines) for all reflecting methods away from the boundary. Near the boundary, the reflection scheme performs the best. For penalization scheme, the particles are pushed inwards and cause a density drop. As for projection scheme, the particles accumulate at the endpoints and cause a density jump. Besides, the potential is shown in Figure 2(Down). It's clear that the boundary layer is $\mathcal{O}(1)$ when $\nu = 1$. Similar simulation results when $\nu = 0.01$ is shown in Figure 3. In the scaling, $Q_+ = 0.4, Q_f = 4\nu, N_+ = 10^5, L = 15, \tau = 0.02\nu$, the boundary layer is roughly 0.1.

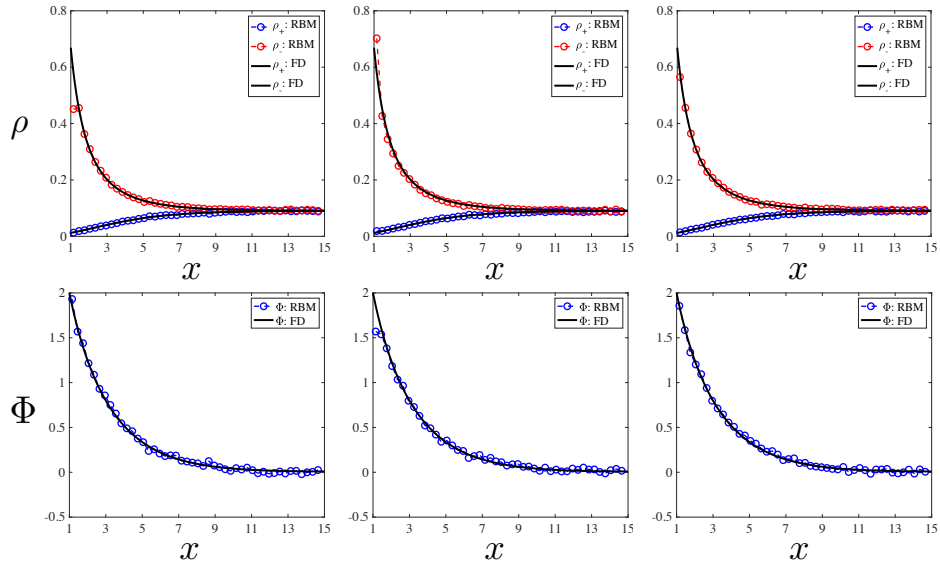


Figure 2: Equilibrium distributions(Up) and potential(Down) when $\nu = 1$. FD vs RBM. Left: penalization; middle: projection; right: reflection.

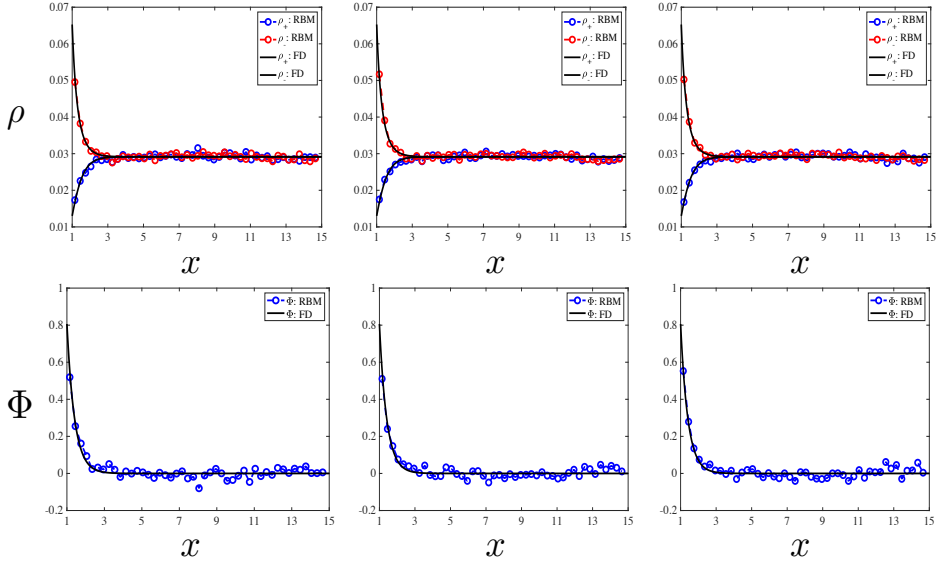


Figure 3: Equilibrium distributions(Up) and potential(Down) when $\nu = 0.01$. FD vs RBM. Left: penalization; middle: projection; right: reflection.

To test the quality of the empirical densities, we test the weak convergence. For a given test function $f(x)$, we compute the estimated expectation for positive and negative charges $\bar{f}_\pm = \frac{1}{N_\pm} \sum_{i \in I_\pm} f(X^i(T))$. The sampling accuracy is measured via the square root of the Mean Square Error (MSE) over M independent repetitive experiments

$$\text{MSE}_\pm^{\frac{1}{2}} := \sqrt{\frac{1}{M} \sum_{m=1}^M \left(\frac{\bar{f}_\pm^{(m)} - \int_{\Omega_L} f(x) \rho_\pm^* dx}{\int_{\Omega_L} f(x) \rho_\pm^* dx} \right)^2}.$$

Here, m means the m -th experiment, ρ_\pm^* is the reference densities solved by FD. We use four test functions $f_1(x) = x$, $f_2(x) = x^2$, $f_3(x) = \cos(x/8)$, $f_4(x) = \exp(-(x - L/2)^2/4)$. We test the weak Monte Carlo error for $\nu = 1$, $\tau = 0.01$, $Q_+ = 1$, $Q_f = 2$, $L = 15$, $M = 100$. The results are shown in Figure 4. It's clear that the RBM simulation is halfth-order, which coincides with the Monte Carlo convergence rate. Since the three reflecting schemes give similar convergence results, we only use reflection scheme in the rest of the paper.

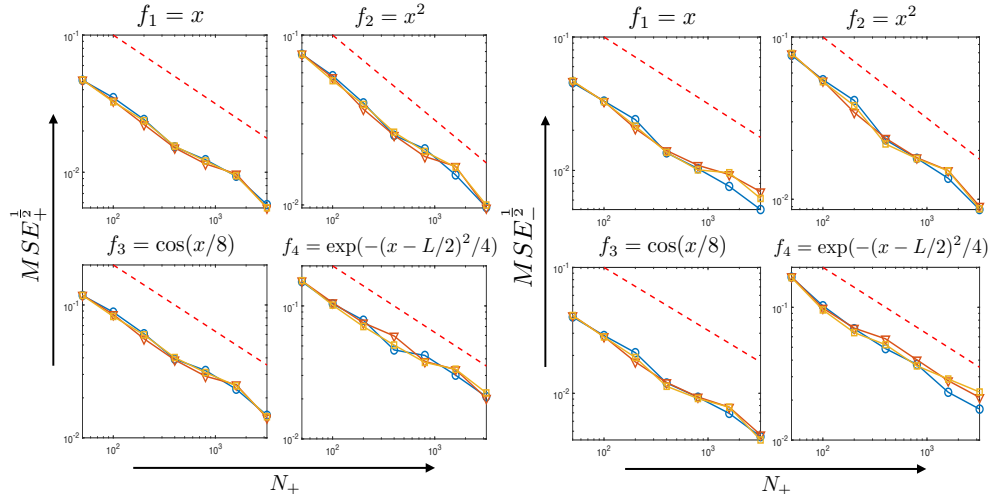


Figure 4: $\text{MSE}_\pm^{\frac{1}{2}}$ error of RBM-PB versus positive particle number N_+ when $\nu = 1$. In each subfigure, the red dashed line denotes the reference slope of $\frac{1}{2}$, the yellow square, red triangle and blue circle represent for penalization, projection and reflection schemes respectively.

In former tests, we check the validity and convergence rate of RBM for PB equation with the total positive charge Q_+ given. Next, consider the problem where ρ_∞ is given instead of Q_+ and test the iterative method proposed in Algorithm 1. Given $\rho_\infty = 0.0218$, fix $\nu = 1$, $L = 30$, $Q_f = 2\nu$, $T_c = 50$, $q = 1e-4$, $\epsilon = 1e-5$, $\tau = 0.1$, one iteration result is shown in Figure 5. After 9 iterations, the RBM simulation reaches the equilibrium state in comparison with the reference FD result. This verifies that the efficient RBM method can also be applied to the case where Q_+ is unknown.

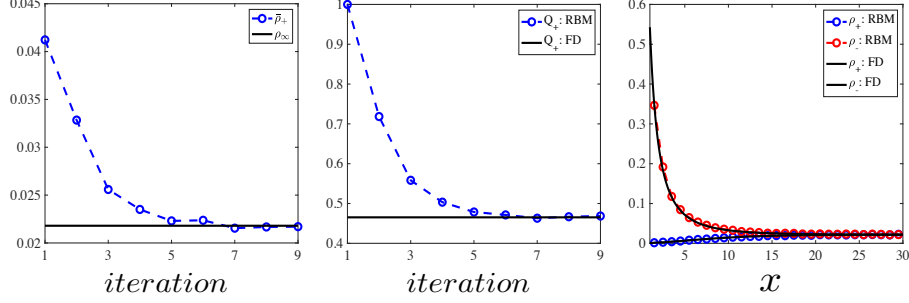


Figure 5: Left: trajectory of $\bar{\rho}_+$; middle: trajectory of Q_+ ; right: equilibrium distributions.

Moreover, this physical model (a charged cell in some electrolyte solution) can be regarded as a capacitor. The differential capacitance is defined by

$$C = \frac{dQ_f}{dV},$$

where $V = \Phi(1) - \Phi(L)$ is the voltage. Figure 6 shows it is feasible to measure the differential capacitance by RBM using iterative Algorithm 1 under different scalings. The concentration of the electrolyte solution, i.e. ρ_∞ , is set to be 0.0218.

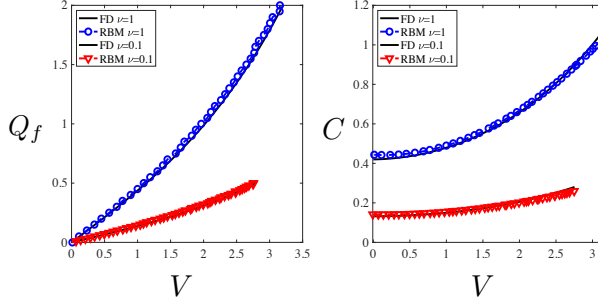


Figure 6: Differential capacitance for 1D example with fixed $\rho_\infty = 0.0218$.

6.2 A 3D example

Assume the cell $\mathcal{C} = \{x \in \mathbb{R}^3 : |x| < R\}$ is a sphere centered at the origin with some positive charge $\rho_f = Q_f \delta(x - x_c)$ in it. Consider a 3D example for symmetric 1:1 salt

$$-\nu \Delta \Phi = \rho_\infty (e^{-\Phi} - e^\Phi), \quad x \in \Omega.$$

As before, we only need to simulate the particles inside a sufficiently large domain $\Omega_L = \{x \in \mathbb{R}^3 : R \leq |x| \leq L\}$. We adopt the splitting strategy introduced in section 4.4.2. The external field here is $E_f(x) = \frac{x - x_c}{4\pi\nu|x - x_c|^3}$.

6.2.1 Spherical symmetric case

When the free charge is in the center of \mathcal{C} , i.e. $x_c = [0, 0, 0]$, the equilibrium distributions of positive and negative charges outside the cell are spherical symmetric. Therefore, the

approximate problem is equivalent to the following

$$\begin{cases} -\nu \ddot{\Phi}_L - \frac{2\nu}{r} \dot{\Phi}_L = \rho_\infty (e^{-\Phi_L} - e^{\Phi_L}), & R < x < L, \\ -\dot{\Phi}_L(R) = \sigma_f, \quad \dot{\Phi}_L(L) = 0. \end{cases} \quad (6.2)$$

Here, “.” means the derivative of r . $\sigma_f = \frac{1}{4\pi R^2 \nu} Q_f$ due to symmetry.

To weaken the random fluctuation, we collect the samples from 100 time steps after the system reaches the equilibrium state. Therefore, we can use relatively small number of particles. The RBM-PB simulation results for $\nu = 1, 0.1, 0.01$ are shown in Figure 7 in comparison with FD. In these tests, $R = 1, L = 10, Q_+ = 20, Q_f = 10\nu, N_+ = 10^4, \tau = 0.01\nu$. Again, RBM-PB can match the FD, which tells RBM is also useful in 3D.

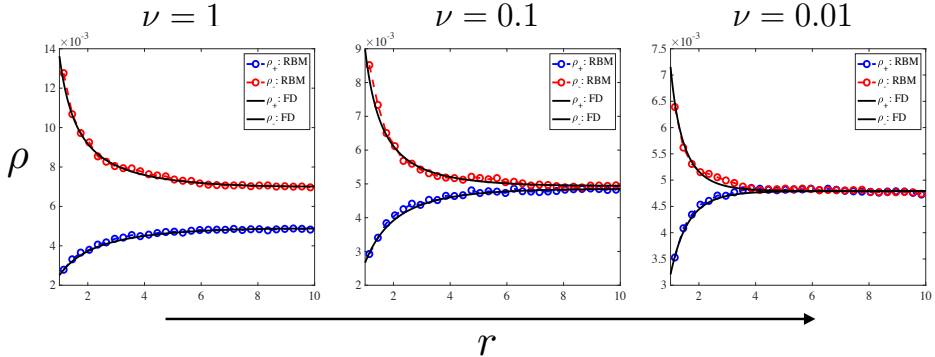


Figure 7: Equilibrium distributions. FD vs RBM. Left: $\nu = 1$; middle: $\nu = 0.1$; right: $\nu = 0.01$.

Similarly, given the ionic concentration ρ_∞ of the electrolyte solution, one can compute the differential capacitance using Algorithm 1 in different scalings. We take $\rho_\infty = 0.005, R = 1, L = 10, q = 1e-3, \tau = 0.01, T_c = 40, \epsilon = 1e-5$. The results for $\nu = 1$ and 0.1 are shown in Figure 8. It is clear that the differential capacitance can be well approximated by RBM-PB for 3D spherical symmetric case.

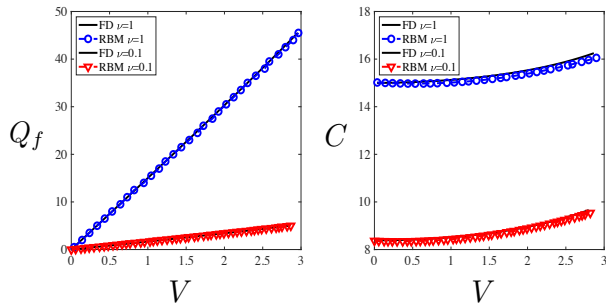


Figure 8: Differential capacitance for 3D spherical symmetric example with fixed $\rho_\infty = 0.005$.

6.2.2 Non-symmetric case

Next, we apply RBM-PB to non-symmetric case. We also collect the samples from 100 different time steps after the equilibrium to get more samples. In order to illustrate the non-symmetry, we plot the projections into different coordinate planes.

Let $x_c = [0, 1.5, 0], R = 2, L = 10, \nu = 1, Q_+ = 10, Q_f = 15, N_+ = 10^4, \tau = 0.01$. In this case, the distributions are not symmetric in the y direction. Since the free charge at x_c is positive, the density of negative charges is higher around x_c due to attraction, while the density of positive charges is lower around x_c due to repulsion. The kernel density estimate in the xOy and yOz planes are shown in Figure 9. We can see that, close to the cell,

the negative charges are more clustered around the free charge while the positive charges are much more sparse around it than elsewhere. Away from the cell, the distributions are approximating radial symmetric. Moreover, both the positive and negative distributions are symmetric in the x and z direction and non-symmetric in the y direction.

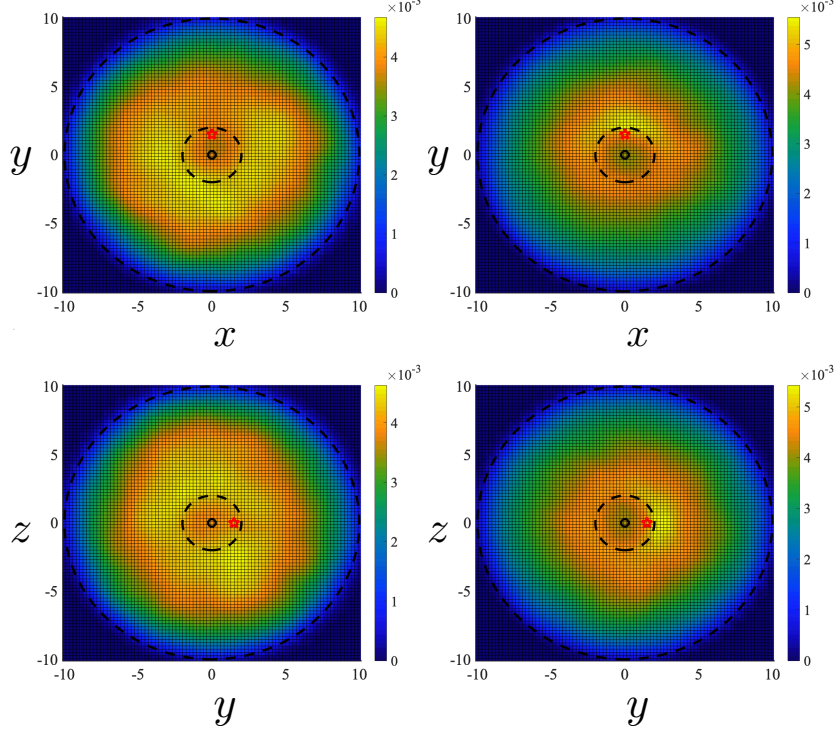


Figure 9: The kernel density estimates in the xOy (Up) and yOz (Down) planes. Left: positive charges; right: negative charges. The black circle and red pentagram represent for the origin and the free charge, the black dashed lines denote the inner and outer boundaries of the truncated domain.

In the spherical coordinates (r, θ, ϕ) , $r(x_c) = 1.5, \theta(x_c) = \pi/2, \phi(x_c) = \pi/2$. One can also observe non-symmetry in the ϕ direction. The kernel density estimates of bulk density in the $r - \phi$ plane are shown in Figure 10. The same colorbar is used in the two subfigures. It is clear that the positive charge density is lower around $\phi = \pi/2$ since the repulsion interaction is stronger than other angles; meanwhile, the negative charge density is higher at $\phi = \pi/2$ due to stronger attraction. In the r direction, the positive charge density is increasing (turning yellow), while the negative charge density is decreasing (turning green).

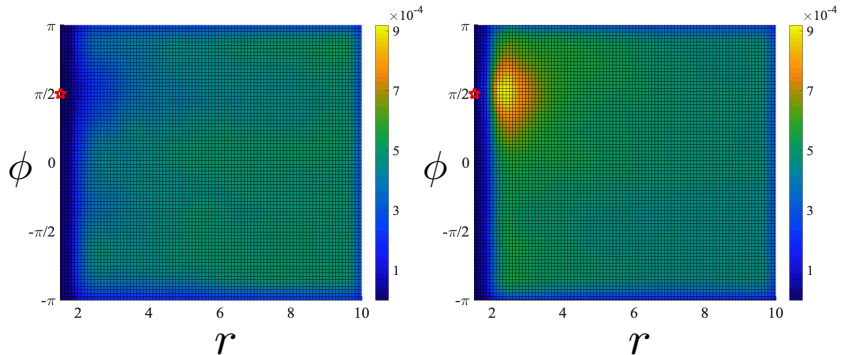


Figure 10: The kernel density estimates in the $r - \phi$ plane. Left: positive charges; right: negative charges. The red pentagram represents for the free charge.

7 Conclusions

In this paper, we proposed a direct simulation approach (RBM-PB) for nonlinear Poisson-Boltzmann equation using the Random Batch Method. At the microscopic level, each ionic particle is subject to the external electric field and interacts with the other $N - 1$ particles through Coulomb potential. By direct particle simulation, we can keep track of the true dynamics of the particle as well as the equilibriums. Meanwhile, the particle method is insensitive to dimension and applicable to complex geometry. Thanks to RBM, the computational cost for interacting particle system is largely reduced from $\mathcal{O}(N^2)$ to $\mathcal{O}(N)$ per time step. Besides, to overcome the difficulty brought by unbounded external domain, we did a truncation and performed the simulation inside the truncated domain. The convergence analysis suggests that such a truncation makes sense. Our numerical results demonstrate that RBM-PB can efficiently simulate the electrostatic distribution of ionic species and capture the screening layer.

Though we only considered the symmetric monovalent electrolyte, this particle method can be easily applied to deal with the case with more than two ionic species. Besides, it is interesting to do simulation for the problem with different dielectric constants in and outside the cell. These are left for future work.

Acknowledgement

The work of L. Li was partially sponsored by NSFC 11901389, Shanghai Sailing Program 19YF1421300 and NSFC 11971314. The work of J.-G. Liu was partially supported by KI-Net NSF RNMS11-07444 and NSF DMS-1812573. Y. Tang would like to thank Prof. S. Jin for his guidance and helpful discussions.

A Discussion about different dielectric constants

In this section, we discuss the effects if the dielectric constant ε inside the cell is different from the one outside.

First of all, recall the classical electrodynamics theory [14]. By Gauss's law,

$$\varepsilon_0 \nabla \cdot E = \rho_F + \rho_p, \quad \rho_p = -\nabla \cdot P,$$

where ε_0 is the dielectric constant in the vacuum, P is the induced electric field, E is the total electric field, and ρ_F , ρ_p and $\rho_F + \rho_p$ represent for the free charge distribution, the induced charge distribution and the total charge distribution respectively. Introducing the electric displacement vector

$$D = \varepsilon_0 E + P = \varepsilon E$$

yields

$$\nabla \cdot D = \nabla \cdot (\varepsilon E) = \rho_F.$$

In other words, the total field E is related to the free charge distribution if we put the varying electricity inside. The effects of induced charge are included in ε .

Suppose that ε is piecewise constant inside and outside the cell \mathcal{C} , i.e.

$$\varepsilon(x) = \begin{cases} \varepsilon_1, & x \in \mathcal{C}, \\ \varepsilon_2, & x \in \Omega. \end{cases}$$

The interface condition on Γ is given by

$$\mathbf{n} \times (E_2 - E_1) = 0, \quad \mathbf{n} \cdot (D_2 - D_1) = 0, \quad (\text{A.1})$$

where we assume there is no free surface charge on the interface. Here, E_1, E_2 and D_1, D_2 are the total electric field and the electric displacement on the interior and exterior side of the cell respectively; \mathbf{n} is the unit normal vector on the interface Γ pointing to Ω . This

means the tangential components of E are continuous on two sides of the matter, while the normal components of E satisfy $\varepsilon_1 E_1 \cdot \mathbf{n} = \varepsilon_2 E_2 \cdot \mathbf{n}$.

We now briefly point out the issue for our problem if ε is different on the two sides. Recall that, in order to solve the equation (2.7), we need to specify the boundary function σ_f according to the free charge distribution ρ_f inside the cell. Unfortunately, if ε is not a constant, this σ_f is not totally determined by the free charge inside the cell. It also includes the induced charge due to the distribution of charges outside the cell. In other words, σ_f is not prescribed in this case and it depends on the solution in the current time. With induced charges counted in σ_f , the interaction between charges in Ω can be given by Coulomb forces.

Alternatively, one can take into consideration the effects of induced charge by solving the Poisson equation with variable ε directly. By Gauss's law, the Poisson equation in the entire space for our problem reads

$$-\nabla \cdot (\varepsilon(x) \nabla \Phi) = e(\rho_f + \sum_{j=1}^J z_j \rho_j), \quad (\text{A.2})$$

where ρ_f is supported in \mathcal{C} and ρ_j is supported in Ω . In order to solve (A.2), one needs to find the fundamental solution of

$$-\nabla \cdot (\varepsilon(x) \nabla \Phi) = \delta(x - x_0), \quad x_0 \in \Omega. \quad (\text{A.3})$$

Clearly, the fundamental solution in Ω is not given by the Coulomb potential

$$\Phi_2(x) = \begin{cases} -\frac{1}{2\pi\varepsilon_2} \ln |x - x_0|, & d = 2, \\ \frac{1}{d(d-2)\alpha(d)\varepsilon_2|x - x_0|^{d-2}}, & d \geq 3, \end{cases}$$

any more. Suppose otherwise. It follows from (A.1) that

$$\varepsilon_1 \nabla \Phi_1 \cdot \mathbf{n} = \varepsilon_2 \nabla \Phi_2 \cdot \mathbf{n}$$

and thus the solution to (A.3) in \mathcal{C} is

$$\Phi_1(x) = \begin{cases} -\frac{1}{2\pi\varepsilon_1} \ln |x - x_0| + C, & d = 2, \\ \frac{1}{d(d-2)\alpha(d)\varepsilon_1|x - x_0|^{d-2}} + C, & d \geq 3, \end{cases}$$

where C is an arbitrary constant. However, a simple computation shows that Φ_1 and Φ_2 violate the continuity of tangential components of E on the interface Γ if $\varepsilon_1 \neq \varepsilon_2$. This makes the problem $-\varepsilon_1 \Delta \Phi = 0$ in \mathcal{C} overdetermined. Therefore, when we apply RBM for variable ε cases directly, the interaction force between two charges outside the cell is no longer Coulomb. However, for some simple regular domain \mathcal{C} (such as sphere domain), the fundamental solution of (A.3) can be obtained by exploiting the image charge method, and the interaction kernel has an explicit formula then. This will be explored in our future work.

B Some missing proofs

Proof of Lemma 5.4. Given $x \in \Omega$. Since $\lim_{|x| \rightarrow \infty} u(x) = 0$, we have

$$\forall \epsilon > 0 \exists L \text{ sufficiently large, } s.t. \quad x \in B_L, \quad |u(x)| < \epsilon \quad \text{for } |x| \in \partial B_L.$$

Let $\Omega_L = B_L \setminus \bar{\mathcal{C}}$. Then

$$\begin{cases} \mathcal{L}u \leq 0, & \text{in } \Omega_L, \\ -\frac{\partial u}{\partial \mathbf{n}} \leq 0, & \text{on } \Gamma, \\ |u| < \epsilon, & \text{on } \partial B_L. \end{cases}$$

By the maximum principle, u attains its nonnegative maximum on $\partial\Omega_L$.

If u attains its nonnegative maximum on $x_0 \in \Gamma$, apply Hopf's lemma, $-\frac{\partial u}{\partial \mathbf{n}} \Big|_{x=x_0} > 0$, this contradicts with $-\frac{\partial u}{\partial \mathbf{n}} \Big|_{\Gamma} \leq 0$. Otherwise, u attains its nonnegative maximum on ∂B_L , so $u(x) \leq |u|_{\partial B_L} < \epsilon$.

By the arbitrariness of ϵ , $u(x) \leq 0$. \square

Proof of Proposition 5.2 in 3D. Throughout this proof, we will denote any generic constants as C , which may change from line to line.

STEP 1: Introduce a function of $s \in \mathbb{R}$,

$$p(s) = \begin{cases} \frac{e^s - e^{-s}}{s} \rho_\infty, & s \neq 0, \\ 2\rho_\infty, & s = 0. \end{cases}$$

Then $p(s) \geq 2\rho_\infty > 0$ is a continuous even function.

So (5.1) can be rewritten as

$$\begin{cases} -\Delta\Phi + p(\Phi)\Phi = 0, & x \in \Omega, \\ -\frac{\partial\Phi}{\partial \mathbf{n}} \Big|_{\Gamma} = \sigma_f, & \Phi(x) \rightarrow 0 \text{ as } |x| \rightarrow \infty. \end{cases}$$

Denote $\Sigma_f = \|\sigma_f\|_{L^\infty(\Gamma)} < +\infty$ and consider the linear problem

$$\begin{cases} -\Delta\bar{\Phi} + 2\rho_\infty\bar{\Phi} = 0, & x \in \Omega, \\ -\frac{\partial\bar{\Phi}}{\partial \mathbf{n}} \Big|_{\Gamma} = \Sigma_f, & \bar{\Phi}(x) \rightarrow 0 \text{ as } |x| \rightarrow \infty. \end{cases} \quad (\text{B.1})$$

By Lemma 5.4, $\bar{\Phi} \geq 0$.

Let $u^\pm = \bar{\Phi} \pm \Phi$, then

$$\begin{cases} -\Delta u^\pm + p(\Phi)u^\pm = (p(\Phi) - 2\rho_\infty)\bar{\Phi} \geq 0, & x \in \Omega, \\ -\frac{\partial u^\pm}{\partial \mathbf{n}} \Big|_{\Gamma} = \Sigma_f \pm \sigma_f \geq 0, & u^\pm \rightarrow 0 \text{ as } |x| \rightarrow \infty. \end{cases}$$

By Lemma 5.4, $u^\pm \geq 0$. That is,

$$|\Phi| \leq \bar{\Phi}, \quad x \in \Omega.$$

STEP 2: In order to express the solution $\bar{\Phi}$ of the exterior Neumann problem (B.1), first construct the interior Dirichlet problem

$$\begin{cases} -\Delta\bar{\Phi} + 2\rho_\infty\bar{\Phi} = 0 & \text{in } \mathcal{C}, \\ \bar{\Phi} = \bar{\Phi}^e & \text{on } \Gamma. \end{cases}$$

Recall that for $x \in \Gamma$, $\bar{\Phi}^e(x)$ and $\bar{\Phi}^i(x)$ represent the limits from exterior and interior side. Hence, $[\bar{\Phi}] = 0$. Then, by the representation formula (5.3), we have

$$\bar{\Phi}(x) = \int_{\Gamma} q(y)G(x-y)dS_y, \quad (\text{B.2})$$

where $q = \left[\frac{\partial\bar{\Phi}}{\partial \mathbf{n}} \right]$ and

$$G(x) = \frac{e^{-\sqrt{2\rho_\infty}|x|}}{4\pi|x|} \quad (\text{B.3})$$

is the three-dimensional Green function.

As for $x \in \Gamma$, $\frac{\partial \bar{\Phi}^e}{\partial \mathbf{n}}(x) = \frac{\frac{\partial \bar{\Phi}^e}{\partial \mathbf{n}}(x) + \frac{\partial \bar{\Phi}^i}{\partial \mathbf{n}}(x)}{2} + \frac{\frac{\partial \bar{\Phi}^e}{\partial \mathbf{n}}(x) - \frac{\partial \bar{\Phi}^i}{\partial \mathbf{n}}(x)}{2}$, q satisfies

$$-\Sigma_f = \int_{\Gamma} q(y) \frac{\partial G(x-y)}{\partial \mathbf{n}_x} dS_y - \frac{q(x)}{2}.$$

Define a kernel $k : \Gamma \times \Gamma \rightarrow \mathbb{R}$ as

$$k(x, y) = 2 \frac{\partial G(x-y)}{\partial \mathbf{n}_x} \quad (\text{B.4})$$

and define an integral operator K by

$$Kf(x) = \int_{\Gamma} k(x, y) f(y) dS_y, \quad x \in \Gamma. \quad (\text{B.5})$$

Then we are led to the Fredholm equation of the second kind:

$$(I - K)q = 2\Sigma_f. \quad (\text{B.6})$$

From Lemma B.1, we know K is compact as operators in $L^2(\Gamma) \rightarrow L^2(\Gamma)$ and also in $C(\Gamma) \rightarrow C(\Gamma)$. $I - K$ is a Fredholm operator. Therefore, given $\Sigma_f \in L^2(\Gamma)$, there exists a unique $q \in L^2(\Gamma)$ such that $(I - K)q = 2\Sigma_f$. Besides, since K is compact in $C(\Gamma) \rightarrow C(\Gamma)$, $q \in C(\Gamma)$. Hence, $\bar{\Phi} \in C^2(\Omega) \cap C(\bar{\Omega})$ from (B.2).

Now we are in a position to show the exponentially decay of $\bar{\Phi}$. For all $x \in \Omega$ satisfying $|x| \geq 2 \sup_{y \in \Gamma} |y|$, it follows from (B.2) that

$$|\bar{\Phi}(x)| \leq \|q\|_{L^2(\Gamma)} \left(\int_{\Gamma} \frac{e^{-2\sqrt{2\rho_{\infty}}|x-y|}}{4^2 \pi^2 |x-y|^2} dS_y \right)^{\frac{1}{2}} \leq \|q\|_{L^2(\Gamma)} \sqrt{|\Gamma|} \frac{e^{-\sqrt{2\rho_{\infty}}|x|/2}}{2\pi|x|}.$$

Thus, there exists $R_1 = 2 \sup_{y \in \Gamma} |y|$ such that

$$|\bar{\Phi}(x)| \leq |\bar{\Phi}(x)| \leq \frac{C}{|x|} e^{-C|x|}, \quad |x| > R_1.$$

Besides, $\Phi \in L^{\infty}(\Omega)$ as $\bar{\Phi} \in C(\bar{\Omega})$.

STEP 3: Look back to the original PB equation (5.1)

$$-\Delta \Phi + 2\rho_{\infty} \Phi = 2\rho_{\infty}(\Phi - \sinh \Phi), \quad x \in \Omega.$$

Let $f := 2\rho_{\infty}(\Phi - \sinh \Phi) \in L^{\infty}(\Omega)$. Then, since $\Phi \in L^{\infty}(\Omega)$, there exists R_2 large enough such that

$$|f(x)| \leq C\Phi^2 \leq \frac{C}{|x|^2} e^{-C|x|}, \quad |x| > R_2. \quad (\text{B.7})$$

Next, by similar arguments with STEP 2, we show the exponentially decay property of $\nabla \Phi$. Construct the interior Dirichlet problem

$$\begin{cases} -\Delta \Phi + 2\rho_{\infty} \Phi = 0 & \text{in } \mathcal{C}, \\ \Phi = \Phi^e & \text{on } \Gamma. \end{cases}$$

Then $[\Phi] = 0$ and by the representation formula (5.3), we have

$$\Phi(x) = \int_{\Gamma} \tilde{q}(y) G(x-y) dS_y + \int_{\Omega} G(x-y) f(y) dy, \quad (\text{B.8})$$

where $\tilde{q} = \left[\frac{\partial \Phi}{\partial \mathbf{n}} \right]$. Similarly, we are led to the Fredholm equation of the second kind

$$(I - K)\tilde{q} = 2(g + \sigma_f) \quad (\text{B.9})$$

with $g = \int_{\Omega} \frac{\partial G(x-y)}{\partial \mathbf{n}_x} f(y) dy \in L^2(\Gamma)$. Therefore, there exists a unique $\tilde{q} \in L^2(\Gamma)$ satisfying (B.9).

Now we estimate the gradient of Φ . One can deduce from (B.8) that

$$\nabla \Phi(x) = \int_{\Omega} \nabla_x G(x-y) f(y) dy + \int_{\Gamma} \nabla_x G(x-y) \tilde{q}(y) dS_y. \quad (\text{B.10})$$

According to (B.3), one has

$$|\nabla_x G(x-y)| \leq \frac{\sqrt{2\rho_{\infty}}|x-y| + 1}{4\pi|x-y|^2} e^{-\sqrt{2\rho_{\infty}}|x-y|}. \quad (\text{B.11})$$

For $x \in \Omega$ satisfying $|x| \geq 2R_2$, consider

$$\begin{aligned} I &:= \int_{\Omega} |\nabla_x G(x-y) f(y)| dy \\ &= \left(\int_{\Omega_1} + \int_{\Omega_2} + \int_{\Omega_3} \right) |\nabla_x G(x-y) f(y)| dy := I_1 + I_2 + I_3, \end{aligned}$$

where $\Omega_1 = \{|x|/2 \leq |y| \leq 2|x|\}$, $\Omega_2 = \{|y| \geq 2|x|\}$, $\Omega_3 = \{|y| \leq |x|/2\} \cap \Omega$. Then, by (B.7) and (B.11), one can obtain that

$$\begin{aligned} I_1 &\leq \|f\|_{L^{\infty}(\Omega_1)} \int_{\Omega_1} |\nabla_x G(x-y)| dy \leq \frac{C}{|x|^2} e^{-C|x|} (2 - (2 + C|x|) e^{-C|x|}) \leq \frac{C}{|x|^2} e^{-C|x|}, \\ I_2 &\leq \|f\|_{L^1(\Omega_2)} \sup_{\Omega_2} |\nabla_x G(x-y)| \leq C e^{-C|x|} \frac{C|x| + 1}{|x|^2} e^{-C|x|} \leq \frac{C}{|x|^2} e^{-C|x|}, \\ I_3 &\leq \|f\|_{L^1(\Omega_3)} \sup_{\Omega_3} |\nabla_x G(x-y)| \leq C|x|^3 \frac{C|x| + 1}{|x|^2} e^{-C|x|} \leq \frac{C}{|x|^2} e^{-C|x|}. \end{aligned}$$

For $x \in \Omega$ satisfying $|x| \geq R_1$, it follows from (B.11) that

$$J := \int_{\Gamma} |\nabla_x G(x-y) \tilde{q}(y)| dS_y \leq \|\tilde{q}\|_{L^2(\Gamma)} \left(\int_{\Gamma} |\nabla_x G(x-y)|^2 dS_y \right)^{\frac{1}{2}} \leq C \frac{C|x| + 1}{|x|^2} e^{-C|x|}.$$

Therefore, there exists a large $R = \max\{R_1, 2R_2\}$ such that for all $|x| \geq R$,

$$|\nabla \Phi(x)| \leq I + J \leq \frac{C}{|x|^2} e^{-C|x|}.$$

□

Lemma B.1. *For smooth boundary $\Gamma \subset \mathbb{R}^2$, the operator K defined by (B.3), (B.4), (B.5) is compact both in $B(L^2(\Gamma))$ and $B(C(\Gamma))$.*

Proof. For compactness in $C(\Gamma) \rightarrow C(\Gamma)$, it is similar to the Laplacian case, and see [15] for the latter.

Now consider the compactness in $L^2(\Gamma) \rightarrow L^2(\Gamma)$:

$$k(x, y) = 2\mathbf{n}(x) \cdot \nabla G(x-y) = \frac{-\mathbf{n}(x) \cdot (x-y)}{2\pi} \frac{\sqrt{2\rho_{\infty}}|x-y| + 1}{|x-y|^3} e^{-\sqrt{2\rho_{\infty}}|x-y|},$$

Since Γ is smooth, $\mathbf{n}(x)$ is almost orthogonal to $(x-y)$ for y close to x , there exists a bounded continuous function $c(x, y)$ such that

$$-\mathbf{n}(x) \cdot (x-y) = |x-y|^2 c(x, y).$$

Thus the kernel is weakly singular (behaves like $|x-y|^{-1}$ as $x \rightarrow y$).

For $\varepsilon > 0$, let

$$k_\varepsilon(x, y) = \frac{c(x, y)}{2\pi} \frac{\sqrt{2\rho_\infty}|x - y| + 1}{|x - y| + \varepsilon} e^{-\sqrt{2\rho_\infty}|x - y|}, \quad x, y \in \Gamma.$$

$$K_\varepsilon f(x) = \int_{\Gamma} k_\varepsilon(x, y) f(y) dS_y, \quad f \in L^2(\Gamma).$$

Then $k_\varepsilon \in L^2(\Gamma \times \Gamma)$, so $K_\varepsilon : L^2(\Gamma) \rightarrow L^2(\Gamma)$ is a Hilbert-Schmidt operator with norm $\|K_\varepsilon\|_{HS} = \|k_\varepsilon\|_{L^2} < \infty$, and hence compact.

Next, we estimate $\|K_\varepsilon - K\|_{B(L^2(\Gamma))}$. For smooth surface Γ , there exist n local charts $D_i \subset \mathbb{R}^2$ and mapping φ_i , $i = 1, \dots, n$ such that

$$\varphi_i \circ k_\varepsilon \sim \frac{C_i|u - v| + C'_i}{|u - v| + \varepsilon} =: \bar{k}_{i,\varepsilon}, \quad \varphi_i \circ k \sim \frac{C_i|u - v| + C'_i}{|u - v|} =: \bar{k}_i, \quad u, v \in D_i.$$

Since $f \in L^2(\Gamma)$, $\bar{f}_i = \varphi_i \circ f \in L^2(D_i)$. Define

$$\bar{K}_{i,\varepsilon} \bar{f}_i(v) = \int_{D_i} \bar{k}_{i,\varepsilon}(u, v) \bar{f}_i(u) du, \quad \bar{K}_i \bar{f}_i(v) = \int_{D_i} \bar{k}_i(u, v) \bar{f}_i(u) du.$$

Let

$$g_{i,\varepsilon}(u) = \frac{C_i|u| + C'_i}{|u| + \varepsilon} 1_{B_i}(u), \quad g_i(u) = \frac{C_i|u| + C'_i}{|u|} 1_{B_i}(u),$$

with bounded sets $B_i \subset \mathbb{R}^2$ s.t. $D_i \subset B_i$, $i = 1, \dots, n$. Then,

$$\bar{K}_{i,\varepsilon} \bar{f}_i = g_{i,\varepsilon} * 1_{D_i} \bar{f}_i, \quad \bar{K}_i \bar{f}_i = g_i * 1_{D_i} \bar{f}_i.$$

Using local charts, it suffices to consider the operators $\bar{K}_{i,\varepsilon}$, \bar{K}_i . Apply Young's convolution inequality, one has

$$\|(\bar{K}_{i,\varepsilon} - \bar{K}_i) \bar{f}_i\|_{L^2(D_i)} \leq \|(g_{i,\varepsilon} - g_i) * 1_{D_i} \bar{f}_i\|_{L^2(\mathbb{R}^2)} \leq \|g_{i,\varepsilon} - g_i\|_{L^1(\mathbb{R}^2)} \|\bar{f}_i\|_{L^2(D_i)}.$$

This implies $\|\bar{K}_{i,\varepsilon} - \bar{K}_i\|_{B(L^2(D_i))} \leq \|g_{i,\varepsilon} - g_i\|_{L^1(\mathbb{R}^2)} \rightarrow 0$ as $\varepsilon \rightarrow 0$ by dominant convergence theorem. Therefore,

$$\|K_\varepsilon - K\|_{B(L^2(\Gamma))} \leq \sum_{i=1}^n \|\bar{K}_{i,\varepsilon} - \bar{K}_i\|_{B(L^2(D_i))} \rightarrow 0 \text{ as } \varepsilon \rightarrow 0,$$

i.e. $K_\varepsilon \rightarrow K$ in $B(L^2(\Gamma))$ as $\varepsilon \rightarrow 0$. Hence, $K : L^2(\Gamma) \rightarrow L^2(\Gamma)$ is a compact operator. \square

References

- [1] G. Allaire, J.-F. Dufrêche, A. Mikelić, and A. Piatnitski. Asymptotic analysis of the Poisson–Boltzmann equation describing electrokinetics in porous media. *Nonlinearity*, 26(3):881–910, 2013.
- [2] N. Baker, M. Holst, and F. Wang. Adaptive multilevel finite element solution of the Poisson–Boltzmann equation; II: Refinement at solvent accessible surfaces in biomolecular systems. *J. Comput. Chem.*, 21(15):1343–1352, 2000.
- [3] A. J. Bordner and G. A. Huber. Boundary element solution of the linear Poisson–Boltzmann equation and a multipole method for the rapid calculation of forces on macromolecules in solution. *J. Comput. Chem.*, 24(3):353–367, 2003.
- [4] D. L. Chapman. A contribution to the theory of electrocapillarity. *Philos. Mag.*, 25:475–481, 1913.
- [5] L. Chen, M. J. Holst, and J. Xu. The finite element approximation of the nonlinear Poisson–Boltzmann equation. *SIAM J. Numer. Anal.*, 45(6):2298–2320, 2007.

- [6] I.-L. Chern, J.-G. Liu, and W.-C. Wang. Accurate evaluation of electrostatics for macromolecules in solution. *Methods Appl. Anal.*, 10(2):309–328, 2003.
- [7] C. M. Cortis and R. A. Friesner. An automatic three-dimensional finite element mesh generation system for the PoissonBoltzmann equation. *J. Comput. Chem.*, 18(13):1570–1590, 1997.
- [8] M. E. Davis and J. A. McCammon. Electrostatics in biomolecular structure and dynamics. *Chem. Rev.*, 90(3):509–521, 1990.
- [9] L. C. Evans. *Partial differential equations. 2nd ed.* American Mathematical Soc., 2010.
- [10] A. Flavell, M. Machen, B. Eisenberg, J. Kabre, C. Liu, and X. Li. A conservative finite difference scheme for PoissonNernstPlanck equations. *J. Comput. Electron.*, 13(1):235–249, 2014.
- [11] M. Gilson, K. Sharp, and B. Honig. Calculating the electrostatic potential of molecules in solution: Method and error assessment. *J. Comput. Chem.*, 9(4):327–335, 1987.
- [12] F. Golse, S. Jin, and T. Paul. The random batch method for N-body quantum dynamics. *arXiv preprint arXiv: 1912.07424*, 2019.
- [13] G. Gouy. Constitution of the electric charge at the surface of an electrolyte. *J. Phys.*, 9:457–468, 1910.
- [14] D. J. Griffiths. *Introduction to Electrodynamics*. Cambridge University Press, 4 edition, 2017.
- [15] W. Hackbusch. *Integral Equations: Theory and Numerical Treatment*, volume 120. Birkhäuser, Berlin, 1995.
- [16] B. Honig and A. Nicholls. Classical electrostatics in biology and chemistry. *Science*, 268:1144–1149, 1995.
- [17] L. Ji, Y. Chen, and Z. Xu. A reduced basis method for the nonlinear Poisson-Boltzmann equation. *Adv. Appl. Math. Mech.*, 11(5):1200–1218, 2019.
- [18] L. Ji, P. Liu, Z. Xu, and S. Zhou. Asymptotic analysis on dielectric boundary effects of modified Poisson–Nernst–Planck equations. *SIAM J. Appl. Math.*, 78(3):1802–1822, 2018.
- [19] S. Jin, L. Li, and J.-G. Liu. Convergence of Random Batch Method for interacting particles with disparate species and weights. *arXiv preprint arXiv: 2003.11257*, 2020.
- [20] S. Jin, L. Li, and J.-G. Liu. Random Batch Methods (RBM) for interacting particle systems. *J. Comput. Phys.*, 400(1):108877, 2020.
- [21] C. Johnson. *Numerical Solution of Partial Differential Equations by the Finite Element Method*. Cambridge University Press, Cambridge, 1987.
- [22] J. E. Jones. On the Determination of Molecular Fields. II. From the Equation of State of a Gas. *Proc. Roy. Soc. Lond. Ser. A*, 106:463–477, 1924.
- [23] C.-C. Lee. The charge conserving Poisson-Boltzmann equations: Existence, uniqueness, and maximum principle. *J. Math. Phys.*, 55:051503, 2014.
- [24] C.-C. Lee, H. Lee, Y. Hyon, T.-C. Lin, and C. Liu. Boundary layer solutions of charge conserving Poisson-Boltzmann equations: One-dimensional case. *Commun. Math. Sci.*, 14(4):911–940, 2016.
- [25] J. E. Lennard-Jones. Cohesion. *Proc. Phys. Soc.*, 43(5):461–482, 1931.
- [26] L. Li, Y. Li, J.-G. Liu, Z. Liu, and J. Lu. A stochastic version of Stein variational gradient descent for efficient sampling. *Comm. App. Math. Comp. Sci.*, 15, 2020.

- [27] P. L. Lions and A. S. Sznitman. Stochastic differential equations with reflecting boundary conditions. *Comm. Pure Appl. Math.*, 37(4):511–537, 1984.
- [28] P. Liu, X. Ji, and Z. Xu. Modified Poisson-Nernst-Planck model with accurate Coulomb correlation in variable media. *SIAM J. Appl. Math.*, 78(1):226–245, 2018.
- [29] J. R. Looker. Semilinear elliptic Neumann problems with rapid growth in the nonlinearity. *Bull. Austral. Math. Soc.*, 74(2):161–175, 2006.
- [30] B. Lu, X. Cheng, J. Huang, and J. A. McCammon. Order N algorithm for computation of electrostatic interactions in biomolecular systems. *PNAS*, 103(51):19314–19319, 2006.
- [31] B. Z. Lu, Y. C. Zhou, M. J. Holst, and J. A. McCammon. Recent progress in numerical methods for the Poisson-Boltzmann equation in biophysical applications. *Commun. Comput. Phys.*, 3(5):973–1009, 2008.
- [32] D. Lpingle. Euler scheme for reflected stochastic differential equations. *Math. Comput. Simul.*, 38:119–126, 1995.
- [33] J.-L. Menaldi. Stochastic variational inequality for reflected diffusion. *Indiana Univ. Math. J.*, 32(5):733–744, 1983.
- [34] R. Pettersson. Approximations for stochastic differential equations with reflecting convex boundaries. *Stochastic Process. Appl.*, 59(2):295–308, 1995.
- [35] A. Pilipenko. *An introduction to stochastic differential equations with reflection*. Potsdam University Press, Potsdam, 2014.
- [36] Y. Saisho. Stochastic differential equations for multi-dimensional domain with reflecting boundary. *Probab. Theory Relat. Fields*, 74(3):455–477, 1987.
- [37] U. Schumann and R. A. Sweet. Fast Fourier transforms for direct solution of Poisson’s equation with staggered boundary conditions. *J. Comput. Phys.*, 75(1):123–137, 1988.
- [38] A. V. Skorokhod. Stochastic equations for diffusion processes in a bounded region. I. *Theory Probab. Appl.*, 6(3):246–274, 1961.
- [39] A. V. Skorokhod. Stochastic equations for diffusion processes in a bounded region. II. *Theory Probab. Appl.*, 7(1):3–23, 1962.
- [40] L. Somiski. Euler’s approximations of solutions of SDEs with reflecting boundary. *Stochastic Process. Appl.*, 94(2):317–337, 2001.
- [41] H. Tanaka. Stochastic differential equations with reflecting boundary condition in convex regions. *Hiroshima Math. J.*, 9(1):163–177, 1979.
- [42] Y. Zhou, W. Cai, and E. Hsu. Computation of local time of reflecting Brownian motion and probabilistic representation of the Neumann problem. *Commun. Math. Sci.*, 15:237–259, 2017.